FANO-CONTROL OF LOCALIZED AND NONLOCALIZED NONLINEAR RESPONSE

LOKALİZE VE LOKALİZE OLMAYAN DOĞRUSAL OLMAYAN SİNYALİN FANO KONTROLÜ

Zafer ARTVİN

Assoc. Prof.Dr. Mehmet Emre TAŞGIN

Supervisor

Submitted to Graduate School of Science and Engineering of Hacettepe University as a Partial Fulfillment to the Requirements for the Award of the Degree of **Doctor of Philosophy** in **Nanotechnology and Nanomedicine**

2020

To my family:Elif, Bahadır and Furkan

ETHICS

In this thesis study, prepared in accordance with the spelling rules of Institute of Graduate School of Science and Engineering of Hacettepe University,

I declare that

- all the information and documents have been obtained in the base of the academic rules,
- all audio-visual and written information and results have been presented according the rules of scientific ethics,
- in case of using other works, related studies have been cited in accordance with the scientific standards,
- all cited studies have been fully referenced,
- i did not do any distortion in the data set,
- and any part of this thesis has not been presented as another thesis study at this or another university.

3./12./ 2020

ZAFER ARTVİN

YAYINLANMA FİKRİ MÜLKİYET HAKKLARI BEYANI

Enstitü tarafından onaylanan lisansüstü tezimin/raporumun tamamını veya herhangi bir kısmını, basılı (kağıt) ve elektronik formatta arşivleme ve aşağıda verilen koşullarla kullanıma açma iznini Hacettepe üniversitesine verdiğimi bildiririm. Bu izinle Üniversiteye verilen kullanım hakları dışındaki tüm fikri mülkiyet haklarım bende kalacak, tezimin tamamının ya da bir bölümünün gelecekteki çalışmalarda (makale, kitap, lisans ve patent vb.) kullanım hakları bana ait olacaktır.

Tezin kendi orijinal çalışmam olduğunu, başkalarının haklarını ihlal etmediğimi ve tezimin tek yetkili sahibi olduğumu beyan ve taahhüt ederim. Tezimde yer alan telif hakkı bulunan ve sahiplerinden yazılı izin alınarak kullanması zorunlu metinlerin yazılı izin alarak kullandığımı ve istenildiğinde suretlerini Üniversiteye teslim etmeyi taahhüt ederim.

Yükseköğretim Kurulu tarafından yayınlanan **"Lisansüstü Tezlerin Elektronik Ortamda Toplanması, Düzenlenmesi ve Erişime Açılmasına İlişkin Yönerge"** kapsamında tezim aşağıda belirtilen koşullar haricince YÖK Ulusal Tez Merkezi / H. Ü. Kütüphaneleri Açık Erişim Sisteminde erişime açılır.

☐ Enstitü / Fakülte yönetim kurulu kararı ile tezimin erişime açılması mezuniyet tarihimden itibaren 2 yıl ertelenmiştir.

☐ Enstitü / Fakülte yönetim kurulu gerekçeli kararı ile tezimin erişime açılması mezuniyet tarihimden itibaren .... ay ertelenmiştir.

☐ Tezim ile ilgili gizlilik kararı verilmiştir.

..3.. / ..12../2020

ZAFER ARTVİN

ABSTRACT

FANO-CONTROL OF LOCALIZED AND NONLOCALIZED NONLINEAR RESPONSE

Zafer ARTVİN

Doctor of Philosophy, Department of Nanotechnology and Nanomedicine

Supervisor: Assoc.Prof.Dr. Mehmet Emre TAŞGIN

November 2020, 100 pages

We investigate the response of nonlinear media interacting with metal nanoparticle-quantum emitter dimers.

First, we study the control of *local* nonlinear processes taking place in a hot-spot. Fano resonances can control nonlinear response in two ways. (i) A linear Fano resonance can enhance the hot spot field, resulting in an enhanced nonlinear signal. (ii) A nonlinear Fano resonance can enhance the nonlinear signal also without enhancing the hot spot. Here, we utilize the latter one, i.e., case (ii). On a basic analytical model, we obtain the steady state solutions for the linear and nonlinear response. We demonstrate the enhancement and suppression of the second harmonic generation (SHG) process. We also compare our results with the numerical solutions to Maxwell equations via finite difference time domain (FDTD) simulations. Most importantly, we demonstrate the suppression of SHG process by utilizing the FDTD simulations which is predicted by the analytical model. The suppression takes place if the level-spacing of the quantum emitter (QE) is chosen to match the SH frequency, i.e., ω_{eg}. Such a phenomenon can be utilized for preventing nonlinear losses.

Second, we study the Fano-control of nonlocal processes, i.e., the ones taking place out of the hot spots. The Fano control of local nonlinear processes in the hot spots has already been studied extensively in the literature. Conventional frequency converters, however, operate throughout the crystal body. Thus, here we study the case where the frequency conversion process takes place along the body of a nonlinear crystal. Metal nanoparticle-quantum emitter dimers control the down-conversion process, taking place throughout the crystal body, via introducing interfering conversion paths. Dimers behave as interaction centers. We show that 2 orders of magnitude enhancement is possible at weak interaction strengths, on top of the enhancement due to localization effects. That is, this factor multiplies the enhancement taking place due to the field localization. Our findings also provide a switch mechanism for the nonlinear conversion via voltage tuning the level spacing of QEs.

Keywords: Fano Resonances, Nonlinear Optics, Second Harmonic Generation, Down conversion and Quantum Optics.

ÖZET

LOKALİZE VE LOKALİZE OLMAYAN DOĞRUSAL OLMAYAN SİNYALİN FANO KONTROLÜ

Zafer ARTVİN

Doktora, Nanoteknoloji ve Nanotıp ABD

Tez Danışmanı:Doç.Dr. Mehmet Emre TAŞGIN

Kasım 2020, 100 sayfa

Metal nanopartikül-kuantum yayıcı dimerler ile etkileşim halinde doğrusal olmayan ortamın tepkisi araştırılmıştır.

İlk olarak, bir sıcak noktada gerçekleşen yerel doğrusal olmayan süreçlerin kontrolünü incelenmiştir. Bu tür yerel Fano rezonanslar, doğrusal olmayan yanıtı iki şekilde kontrol edebilir.(i) Doğrusal Fano rezonans, sıcak nokta alanını geliştirerek doğrusal olmayan sinyalin artmasına neden olabilir.(ii) Doğrusal olmayan bir Fano rezonans, sıcak noktayı güçlendirmeden doğrusal olmayan sinyali geliştirebilir. Burada, ikincisini, yani durum (ii)'yi kullanılmıştır. Analitik model ile kararlı durumlarda doğrusal ve doğrusal olmayan sinyal için sonuçlar elde ettik. Bu sonuçlarda ikinci harmonik üretim (SHG) sürecinin geliştirilmesi ve bastırılması gösterilmiştir. Ayrıca Maxwell denklemlerinin sayısal çözümü ile elde edilen sonuçlarımız sonlu fark zaman alanı (FDTD) simülasyonları ile karşılaştırıldı. Analitik model tarafından tahmin edilen SHG sinyalinin bastırılmasını FDTD simülasyonları ile gösterilmiştir. Baskılanma, kuantum yayıcının (QE) seviye aralığı SH frekansıyla eşleşecek şekilde seçilirse gerçekleşir, yani ω_{eg}. Böyle bir fenomen, doğrusal olmayan kayıpları önlemek için kullanılabilir.

İkinci olarak, yerel olmayan süreçleri, yani sıcak noktalarda meydana gelen Fano-kontrolünü inceliyoruz. Sıcak noktalardaki yerel doğrusal olmayan süreçlerin kontrolü, literatürde kapsamlı bir şekilde incelenmiştir. Bununla birlikte, geleneksel frekans dönüştürücü doğrusal olmayan kristaller, tüm kristal boyunca frekans dönüşümü yaparlar. Bu nedenle, burada, frekans dönüştürme işleminin doğrusal olmayan bir kristalin gövdesi boyunca gerçekleştiği durumu inceliyoruz. Metal nanopartikül-kuantum yayıcı dimerleri, engelleyici dönüşüm yolları sunarak, kristal gövde boyunca gerçekleşen aşağı dönüşüm sürecini kontrol eder. Dimerler etkileşim merkezleri gibi davranırlar. Zayıf etkileşim güçlerinde, yerelleştirme etkilerinden kaynaklanan artışın yanı sıra, 2 dereceli bir artışın mümkün olduğunu gösterilmiştir. Bu faktör, alan lokalizasyonu nedeniyle meydana gelen artış ile çarpılır. Bulgularımız ayrıca, QE'lerin seviye aralıklarını elektrik alan ile kontrol edilmesi doğrusal olmayan dönüşüm için bir anahtar mekanizmasının mümkün olduğunu gösterir.

Anahtar Kelimeler: Fano rezonansları, Doğrusal olmayan optik, ikincil harmonik üretim, aşağı çevrim ve kuantum optik

THANKS

I would first like to thank my supervisor Assoc. Prof.Dr. Mehmet Emre Taşgın, whose expertise was invaluable in guiding me at research and methodology.

I would also like to thank my thesis advisory committee members Prof. Dr. Haluk Utku and Assoc. Prof.Dr. Alpan Bek for their guidance and contributions. I also want to thank to Dr. Mehmet Günay for his collaborations and guidance.

Finally, I could not have completed this thesis without the support of my family. I would like to thank my Elif, Bahadır and Furkan.

Contents

List of Tables

List of Figures

SYMBOLS AND ABBREVIATIONS

SYMBOLS f_i Interaction strentghs between MNP and driving field

f_c Interaction strentghs between MNP and QE

g Interaction strentghs between MNP and crystal cavity mode

a_i Nonlinear crystal cavity modes

γ_i Decay rates of the cavity modes

$\gamma_{ee,eg}$ Decay rates of quantum emitter

P Polarization density

χ Linear susceptibility

$\chi^{(2)}, \chi^{(3)}$ Second and third order nonlinear susceptibilites

E Electric field

ABBREVIATIONS

EM Electromagnetic

MNP Metal Nano Particle

LSP Localized Surface Plasmon

SHG Second Harmonic Generation

SPDC Spontaneous Parametric Down Conversion

PDC Parametric Down Conversion

FR Fano Resonance

QE Quantum Emitter

QD	Quantum Dot
3D	Three Dimensional
FDTD	Finite Difference Time Domain
THG	Third Harmonic Generation
SERS	Surface Enhanced Raman Spectroscopy
FWM	Four Wave Mixing
BEM	Boundary Element Method

1 INTRODUCTION

Interaction of high intensity light with matter makes nonlinear processes visible. The material's optical properties can be modified by the presence of the strong electromagnetic (EM) waves and this leads to nonlinear optical effects such as the Kerr effect, self-focusing, optical solitons, high-harmonic generation and down-conversion of light [1]. Observation of some optical effects necessitates the use of high-intensity sources or locally enhanced hot spots. Using the current nanotechnological methods, it is possible to fabricate nanostructures, like metal nanoparticles (MNPs), trapping incident radiation into nanometer-sized "hot spots", as localized surface plasmon (LSP) oscillations. The intensity of the hot spots (the near field) can be 10^5 times of the one for the incident field [2, 3] or even further [4].

This phenomenon enables several technical applications which are based on the enhancement of linear and nonlinear responses. Localization also strengthens the nonlinear properties of molecules positioned in the vicinity of the hot spots. For instance, signal from a Raman-reporter molecule can be enhanced remarkably [5]. Similarly, nonlinear processes like second harmonic generation (SHG) [6], four wave-mixing (FWM) [7] and down conversion processes [8, 9, 10] are also enhanced.

The field-localizing feature of the metal nanostructures not only enhances the nonlinear processes, but also leads to an enhanced light-matter interaction at the hot spots of MNPs. Quantum emitters (QE), located at the hot spots, strongly couple to the near-field (polarization) generated by the plasmonic excitations. Such couplings can be several orders of magnitude greater than the direct coupling of a QE to the incident light. Strong interaction between a QE and a metal nanoparticle (MNP) makes path interference effects visible. These are called as Fano resonances [11], the plasmon-analogue of the phenomenon electromagnetically induced transparency (EIT) [12]. Similar to EIT-like behaviors in atomic clouds [12], Fano resonances can be used to control the refractive-index [13, 14, 15] and nonlinear conversion processes [16, 17, 18]. The origin of these interference effects, e.g., enhancement and suppression of linear and/or nonlinear response, can be demonstrated with a basic analytical model. Cancellations in the denominator of a converted amplitude result in enhancement of the processes [19, 20, 17]. Besides providing such control methods on the steady-state amplitudes, the lifetime of plasmon oscillations can also be extended by Fano

resonances [21, 22, 23, 24, 25, 11], at the hot spots, leading to a further amplification of the field strength, i.e., dark-hot resonances [26, 27, 28]. The same incident field intensity, a MNP with an FR can accumulate more intense field at the hot spot. This enhancement in the plasmon lifetime enables the operation of spasers [29, 30], nano-lasers. Dark-hot resonances appear strongest when the incident field is resonant to the transparency window [26]. In a nonlinear process both incident and the generated fields are enhanced. Also such kind of Fano resonances, extending the plasmonic lifetime, further enhances both incident and generated fields. Actually, it is ironical that a Fano resonance enhances the lifetime of plasmons in short-time dynamics, while it suppresses the excitations (also conversion) in the steady-state.

In this thesis, I work on the steady-state control of nonlinear processes. First, (i) I study a local nonlinear (second harmonic generation, SHG) process taking place at a hot spot [31]. Then, (ii) I study the control of *unlocalized* processes taking place in the body of a frequency converting crystal. In particular, we are interested with the control of spontaneous down conversion via utilizing MNPs as interaction centers.

(i) While SHG can be utilized in many applications such as in all optical switching [32] and in achieving quantum states [33] it is an undesired process in, e.g., optical fibers. The nonlinear frequency generation can cause losses in the fundamental (first harmonic frequency) signal [34]. Thus, a mechanism for controlling SHG taking place at the hot spots, is beneficial. The SHG signal can be adjusted both by controlling the linear response and the nonlinear response.

In Chapter 3, we study on gaining control over the steady state of second-harmonic signal via path interferences (a) in the linear and (b) nonlinear responses. We show that steady-state SHG, taking place at a hot spot, can be enhanced by controlling the linear signal. In method (b), Fano resonance in the nonlinear response, we show how to control (both enhance and suppress) the SHG without altering the linear response, i.e., the hot spot field. We compare our analytical results with the exact solution of Maxwell equations obtained by finite difference time domain (FDTD) simulation. The two solutions match quite successfully. In particular, we demonstrate that the SHG suppression, predicted by an analytical model, is observable in the FDTD simulations.

Such plasmonic path interference effects, where the nonlinear conversion process takes place on a local region, have already been studied extensively. In these setups both the generation of the nonlinear (up or down conversion) field and the interaction of the quantum emitter with such a nano-converter take place at the hot spot. In systems, where nanoparticles are embedded into nonlinear crystals [8, 9, 10, 35], however, nonlinear process takes place all over the crystal body, i.e., not merely on the nanoparticle hot spot.

(ii) Actually, it is more important to achieve control over *unlocalized* nonlinear processes. The path interference effects discussed so far, both above and in the literature [16, 17, 18], control a nonlinear processes taking place at the hot spot of a metal nanostructure. In the conventional frequency converters, however, the nonlinear process takes place along the body of a nonlinear crystal [36]. Such crystals are demonstrated to generate enhanced nonlinear signal when embedded with MNPs [8, 9, 10, 35]. The enhancement appears due to field localization around the MNPs. Fano-control in such crystals, however, has not been considered yet.

In this thesis, we also study how path interferences induce in such a system [**?**]. Spontaneous parametric down conversion (SPDC) or down conversion (DC) generates entangle photon pairs. Thus, such sources play a key role in quantum optics implementations. The entanglement can be in polarization, space, time and orbital angular momentum degrees of freedom. Generating of entangled beam/photon pairs are essential for many quantum optics applications [37]. It is a key resource in quantum communication including cryptography [38], quantum computation [39] and quantum information [40]. Down conversion (DC) can also be used in solar cell applications by means of harvesting high frequency spectrum by converting high energy photons into two or more lower energy photons [41, 42].

Despite presenting such an important role in various applications in quantum technologies [43, 44, 45], limited efficiencies of nonlinear materials in parametric down conversion process, i.e., the conversion rate, still poses a disadvantage in technological applications [37] (only one photon out of 10^8 undergoes conversion [46]). Some recent works [47, 48] report on improvement of the conversion efficiency via changing the geometry/structure of the nonlinear crystals. Further nonlinearity enhancements are achieved by MNP-embedding into the nonlinear crystals [8, 9, 10, 35]. In such systems, however, once the MNPS are embedded; a tuning of frequency conversion is not achievable. Thus, here, we present a parametric down

converting crystal whose conversion can be tuned via an applied voltage.

In Chapter 4, we study the nonlinear response of a down-converting crystal whose surface is decorated with MNP-QE dimers. The level-spacings of the QEs (ω_{eg}) are tunable via applied voltage. The MNPs behave as interaction centers. They make the unlocalized down-converted field concentrate into the hot spots where a stronger interaction with the quantum emitter takes place, e.g., compared to QE-embedded crystals [8, 9, 10, 35]. We show that such a setup can enhance the down-converted field 2 orders of magnitude with quite weak interaction strengths. It should be emphasized that, this enhancement comes as a further multiplication factor on top of the MNP hot spot enhancement.

The findings of Chapter 3 and Chapter 4 based on our following publications: "Controlling steady-state second harmonic signal via linear and nonlinear Fano resonances" Journal of Modern Optics (2020) [31] and "Fano-control of down-conversion in a nonlinear crystal embedded with plasmonic-quantum emitter hybrid structures" accepted by Journal of Optical Society of America B (2020) [49].

2 BACKGROUND INFORMATION

In this section, we briefly introduce the basic concepts such as plasmons, quantum emitter, nonlinear optics, second harmonic generation, parametric down conversion and Fano resonances.

2.1 Plasmons

Surface plasmons or Surface plasmon polaritons (SPP) are oscillations (waves) of the charge density propagating at the surface of the metal and dielectric interfaces (Fig. 2.1a). These oscillations can also form standing waves on the surface of metallic nanoparticles referred as localized surface plasmons (LSP) (Fig. 2.1b). Localization of surface plasmon at MNPs can give rise to strongly enhanced (up to factor 10^5) optical near fields which are spatially confined well below the diffraction limit (half-wavelength) near the MNP's surface [2]. This property has led to a wide range of application for surface plasmons including extreme light concentration and increment of the nonlinear refractive index of materials [1]. The amplitude of surface plasmons decays exponentially with the distance typically in a few hundreds of nanometers into dielectric media from the interface [50].

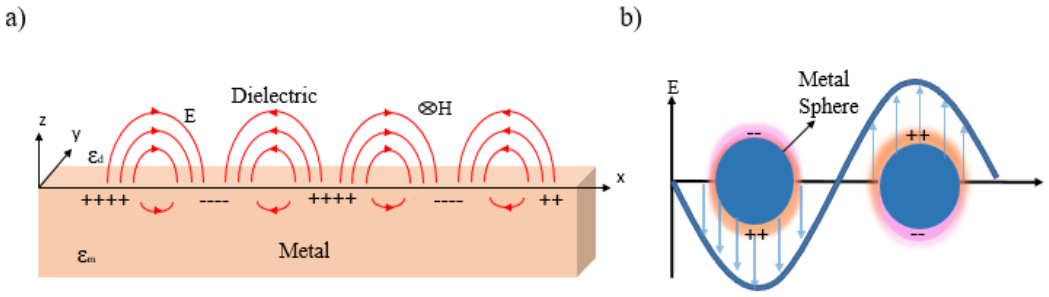

Figure 2.1: a) Surface Plasmons at metal-dielectric interface b) formation of localized surface plasmons (LSPs) at metal nanoparticle excited by free-space EM wave. Figures adapted from Ref. [50]

In metal nanoparticles, the response to the optical excitations arises from the localized surface plasmons (LSPs), whose resonances depend on size and shape of the nanoparticle. Additionally, nano-antennas, plasmonic metamaterials, waveguides can be used together to customize the optical response through their electromagnetic couplings.

An enhanced nonlinear optical response can be obtained by using the plasmonic effects. The nonlinear response of the materials, e.g., nonlinear crystals, can be weak. The nonlinear conversion rates depend on the electromagnetic field strength, which can be enhanced by designing the materials by utilizing the plasmonic effects.

2.2 Quantum emitters

Quantum emitters, e.g., quantum dots, molecules and defect (color) centers at diamonds are used as single-photon sources. They generate quantum light for many scale-able quantum technological applications including quantum computing, quantum communication, quantum cryptography [51].

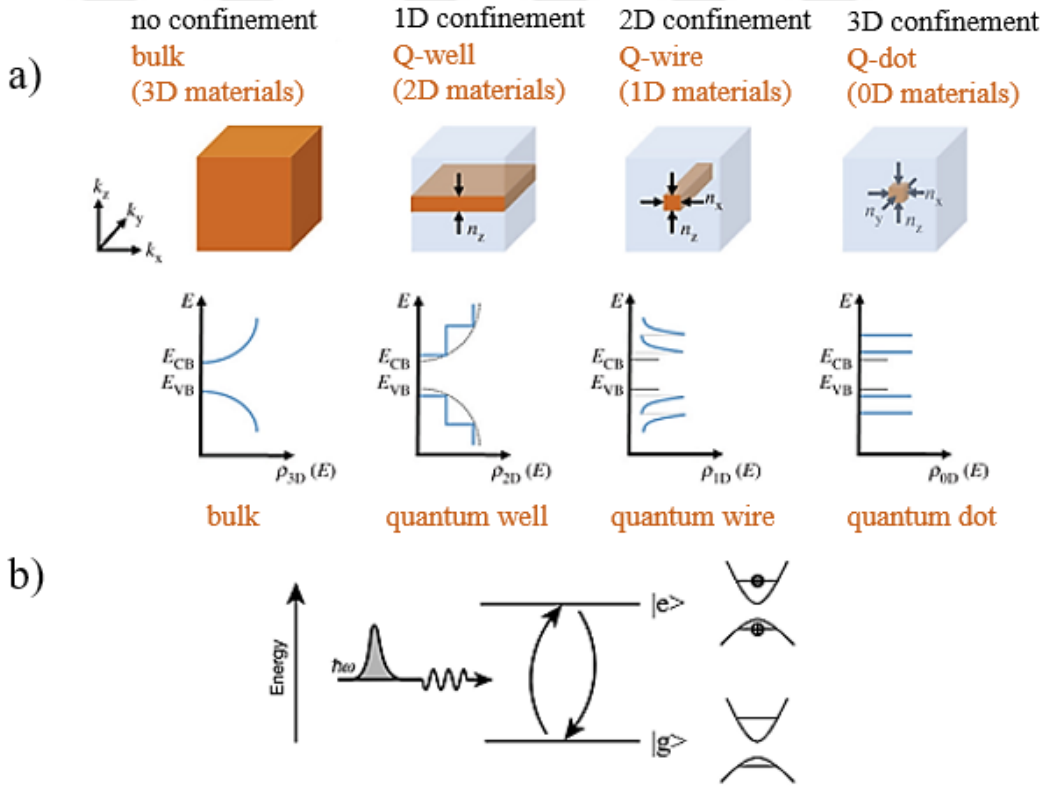

Figure 2.2: a) Energy diagrams and density states for 1D, 2D and 3D confined materials. b) Schematic view of a two-level system. The state $|g>$ corresponds to ground state and $|e>$ corresponds to excited state (Figures adapted from a) Ref. [46] and b) Ref. [45])

As the structure sizes go down to nanometer scale, the discretization of the energy levels becomes more and more apparent and results in changes in the optical and electronic

properties of the materials [52], Fig. 2.2a. In a quantum dot, the movement of electrons is confined in all three dimensions. Energy difference between valence band and conduction band increases with smaller QD dimensions. These zero-dimensional materials are often referred as artificial two level atoms, Fig 2b. Quantum dots are treated as be two level systems with ground state $|g>$ (lower energy state) and excited state $|e>$ (upper energy state). It is possible to transit between these states by inducing resonant driving field, which has the similar energy with the level spacing [51]. Level spacing corresponds to the energy difference between the upper and the lower states which can be represented in terms of frequency. The level spacing frequency depends on the type and the size of the molecule and can also be tuned with an external electric field (applied voltage) [53, 54].

QDs have sharp fluorescence emission peaks and consequently higher radiative lifetimes. The typical lifetime of the quantum dots is around a few nanoseconds and which is orders of magnitude larger compared to the surface plasmons, typically $10^{-14} - 10^{-13}$s. Because of the lifetime difference between QDs and MNPs, Fano resonances can be observed also in MNP-QE dimer structures [3].

2.3 Nonlinear crystals

Nonlinear crystals are transparent crystalline materials which can be used to convert the incoming frequency of photons to higher or lower frquebcies. The polarization density (P) nonlinear crystals reacts nonlinearly to the electric field (E) of the incident EM radiation. Nonlinear crystals are electromagnetic media which can exhibit second $\chi^{(2)}$ and/or third $\chi^{(3)}$ order polarizations, which converts the incident light into other frequencies. Because of the low conversion rates, i.e., small $\chi^{(2,3)}$ factors, powerful light sources (high-intensity lasers) are needed to observe the nonlinear response. Various types of conversion processes for the incident light (multiplication, division and mixing) is possible in nonlinear optical crystals [36].

There is a wide variety of nonlinear crystals, that can be selected according to the intended use. For the frequency conversion of laser sources, β-barium borate (BBO) and lithium triborate (LBO) nonlinear crystals are mostly used due to their large optical nonlinearities [36].

2.4 Nonlinear Optics

Frequency conversions of the incoming photons/beam, e.g., doubling tripling or splitting the energy, is the subject of *Nonlinear Optics*. Nonlinear optics is a leading and progressive area of research that incorporates new laser technical advantages, photonics, biophotonics, optical sensing and spectroscopy. The linear response of the material is given by

$$P = \epsilon_0 \chi E \tag{2.1}$$

for linear interactions.

The dipole moment per unit volume (Polarization density) depends on the linear susceptibility (χ) of the material and the strength of the applied electric field (E) (ϵ_0 is the permittivity of free space).

The induced polarization depends linearly on the electric field in the case of traditional (i.e. linear) optics. Whereas, in nonlinear optics, the optical reaction can also be defined by generalizing Eq. 2.1 by representing the polarization (P), with the electric fields with higher-order powers

$$P = \epsilon_0[\chi E + \chi^{(2)} E^2 + \chi^{(3)} E^3 + ...] \tag{2.2}$$

$$P = P^{(1)} + P^{(2)} + P^{(3)} + ..., \tag{2.3}$$

where the quantities $\chi^{(2)}$ and $\chi^{(3)}$ are the second and third-order nonlinear optical susceptibilities which determine the strength of the nonlinear response of the material.

A large number of frequency conversion processes can take place in a nonlinear crystal. We will consider the second harmonic generation (SHG) and the spontaneous parametric down-conversion (SPDC) in this thesis.

2.4.1 Second Harmonic Generation

Second-harmonic generation (SHG), is a nonlinear optical process, in which two photons are 'combined' to form a new photons having the twice frequency of the initial photons interacting with the nonlinear material. The SHG of light is used for high-resolution optical microscopy and for characterizing organic or inorganic crystals [55].

SHG was firstly demonstrated by Franken and his colleagues in 1961 [56]. After the discovery of laser sources in 1960 by Maiman [57] experimental study of nonlinear optics became more practical. As the power density of laser sources (novel laser sources have a power density of 10^{12} to 10^{18} W/cm^2) increases, the importance and applications of higher harmonic generation gained more significance [58].

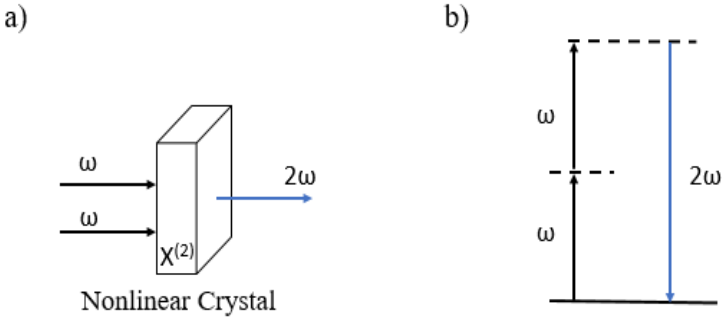

Figure 2.3: a) Illustration of SHG from a nonlinear crystal. b) Energy conversion in a SHG process: energy level diagram.

2.4.2 Spontaneous Parametric Down Conversion

Spontaneous parametric down conversion (SPDC) can be thought to be as an inverse process to the SHG. After theoretical description at 1966 by Klishko, the PDC is experimentally observed. PDC, a second-order nonlinear process, splits an incident beam into two subfrequencies labelled as signal and idler [1]. The generation of the down converted photons takes place inside a nonlinear crystal without any external stimulation (spontaneous). The down conversion process depends not only on the pump and generated field intesities, but also on the phase of the fields. The conversion rate for the down conversion process is at its maximum when the sum of the energies and the momentum of the signal and the idler photons are equal to the ones of pump (Eq. 2.4 and 2.5). This situation is also referred to as "phase-matching" condition.

The input and output frequencies need to match as

$$\omega_p = \omega_s + \omega_i \tag{2.4}$$

A photon of frequency ω_p break down into two photons of lower frequencies which can differ either in the direction or the magnitudes of their wave vectors $\vec{k_s}, \vec{k_i}$, or both. The

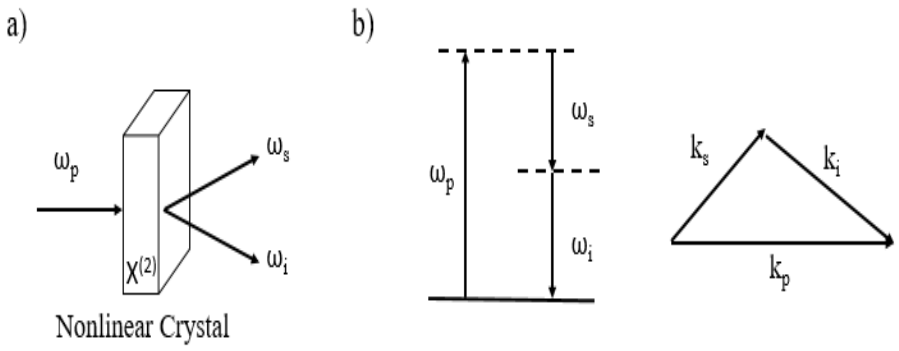

Figure 2.4: SPDC process, The nonlinear crystal photon of frequency ω_p splits into two photons at frequencies ω_s and ω_i b) Energy and momentum conservation in SPDC.

signal-photon frequency ω_s and idler-photon frequency ω_i are traditionally associated with the ranges $\omega_p > \omega_s \geq \omega_p/2$ and $0 < \omega_i \leq \omega_p/2$. The phase-matching condition can be written, for the wave vectors $\vec{k_p}, \vec{k_s}, \vec{k_i}$ of the pump, signal and idler photons as

$$\vec{k_p} = \vec{k_s} + \vec{k_i} \tag{2.5}$$

which is the condition for momentum conservation. At the "phase-matching" condition, the conversion efficiency reaches its maximum value.

PDC is an important process in quantum optic applications, i.e., the down-converted signal and idler photons become indistinguishable quantum objects and constitutes the so-called entangled state. The state is described by a superposed wave function and has several nonclasscical features [59, 60].

2.4.3 Quantum Entanglement

The quantum entanglement is a quantum mechanical phenomenon. The quantum states of two subsystems correlated and the states of subsystems can not be described independently even they are spatially separated. The entangled states cannot be simulated by classical correlations [61].

Parametric down-conversion can produce these entangled states in Bell-EPR state basis. These states have remarkable properties; namely, the result of the measurements for both

subsystems are correlated with a spooky action. Along the two directions ("A" and "B") depicted in Fig. 2.5, where the cones overlap, the light can be essentially described by an entangled state

$$|\psi^{\pm}>=\frac{1}{\sqrt{2}}(|H_1>|V_1>\pm|H_2>|V_1>),$$
$$|\phi^{\pm}>=\frac{1}{\sqrt{2}}(|H_1>|H_2>\pm e^{i\alpha}|V_1>|V_2>), \tag{2.6}$$

where H and V indicate horizontal (extraordinary) and vertical (ordinary) polarization, respectively. The relative phase α arises from the crystal birefringence. An overall phase is omitted.

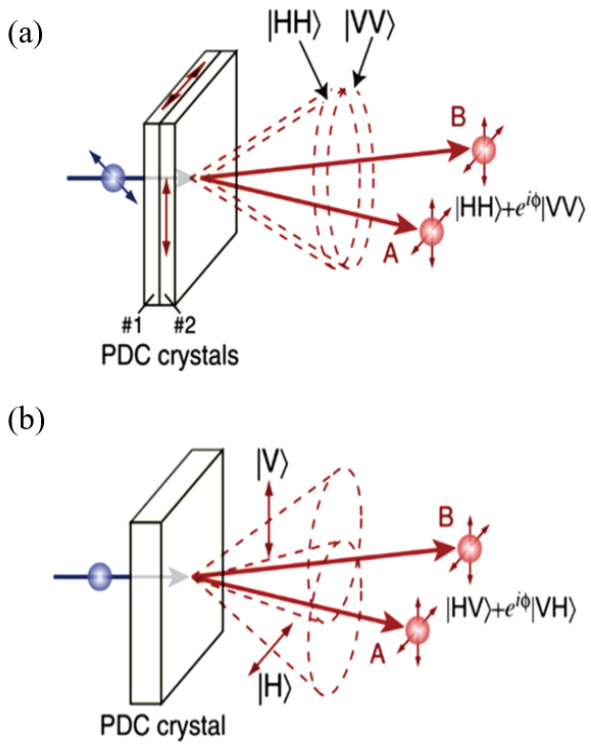

Figure 2.5: Schematic of SPDC generated by pump laser a) Type I: signal and idler photons have same polarization b) Type II: signal and idler photons have orthogonal polarization. Entangled states are generated and can be detected at the directions A and B in both types. Figure is adapted from Ref. [60].

The down-conversion process can entangle two down-converted beams/photons in various degrees of freedom: such as continuous-variable, polarization, space, time and orbital angular momentum [62]. Entangled beam/photon pairs are essential for many fundamen-

tal quantum optics experiments [37] as well as a key resource in quantum communication including cryptography [38], quantum computation [39] and quantum information [40].

2.5 Fano Resonances

"*The interference of a discrete auotoionized state with a continuum gives rise to characteristically asymmetric peaks in the excitation spectra.*" U.Fano.

These asymmetric lineshapes are named as Fano resonances after Ugo Fano at 1961 [63]. Observation of Fano lineshape depends on the discrete quantum state frequency which lies within the continuous frequency range. The plasmons at the surface of a MNP normally have a very short lifetime, $10^{-13}s$ or $10^{-14}s$, compared to QDs, which is typically $10^{-9}s$. Hence, they behave as discrete and continuum states and, their interaction leads to Fano resonances. The spectral line shapes (Fig. 2.6) for the Fano resonances are given by the following equation [64]

$$\sigma_e \approx \frac{[q + (\omega - \omega_0)/\gamma]^2}{1 + (\omega - \omega_0)/\gamma)^2}, \tag{2.7}$$

where q is the Fano parameter which determines the asymmetry level, γ is the resonance width, and ω and ω_0 correspond to frequencies of the continuum and discrete states, respectively.

The Fano formula (2.7) can be employed to interpret resonance shape for a wide range of systems, including plasmonic nanoantennas [65], optomechanical resonators [66], semiconductor nanostructures [67], photonic crystals [68] dielectric nanoparticles [66], and many others. In nanophotonics, the Fano resonance initially been introduced and observed in plasmonic structures. However, plasmonics suffers from high ohmic losses and overheating of structures in many optical devices. Therefore, study of all-dielectric metamaterials [69, 70], with considerably lower losses, and also metasurfaces, which are two-dimensional (2D) successors of metamaterials [71, 72] gained attention by research groups [64] for Fano resonances.

Electromagnetically induced transparency (EIT) is also a path interference effect as Fano

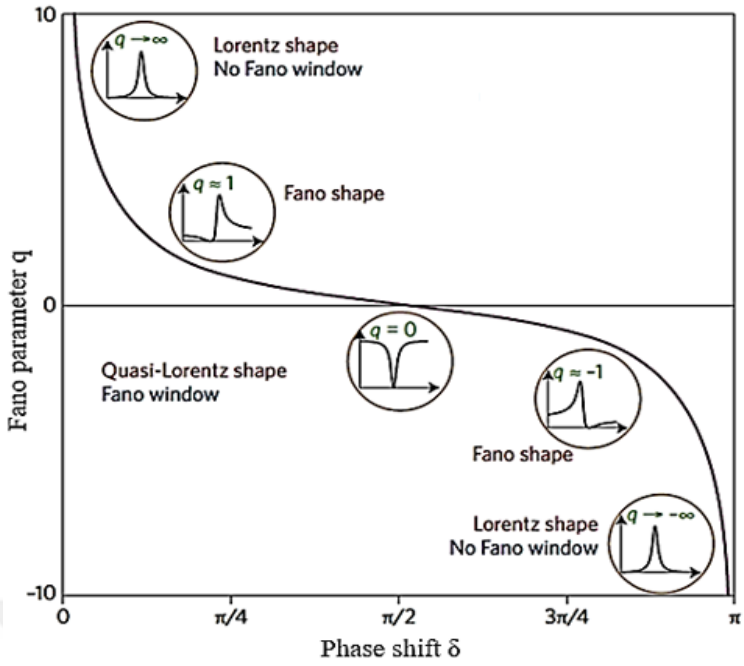

Figure 2.6: Fano lineshapes for different Fano parameters and phase shifts δ between the oscillators. Figure adapted from Ref. [63]

resonances. In EIT the principle energy level is weakly hybridized into two separate energy levels. These two weakly hybridized energy levels depend on the broadening of the excited state ($\gamma_{eg} \sim 10^9$ Hz for a the quantum dot, $\gamma_p \sim 10^{13}$Hz- 10^{14}Hz for plasmon excitation) [25, 73]. The two paths work out of phase with each other. While one path absorbs the incoming radiation, the other one radiates it. This effect displays itself in the form of a dip in absorption spectrum Fig 2.8, alternatively a transparency window.

The main difference between FR and EIT is that Fano resonance in a passive medium and EIT takes place in an active medium. In EIT, a powerful microwave pump can induce weak hybridization of the stimulated energy level. In difference to EIT, Fano resonance does not require the presence of such a driving field, such as a microwave radiation. In Fano resonance a long lifetime object (quantum object or a dark plasmon state) is placed in the hotspot of the MNP. The MNP's own plasmon near-field induces the interaction of the MNP and the auxilary object. In this way, a driving field is not needed.

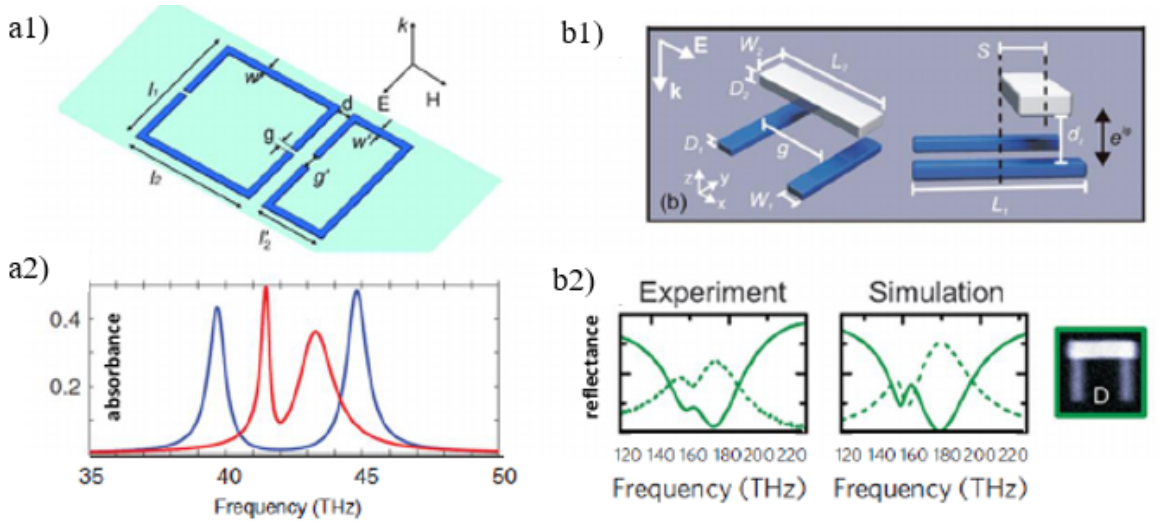

Figure 2.7: Experimental studies to demonstrate the Fano resonances. (a) Split ring resonators structures operate in THz frquency regime [73] (b) The structures consist of nano rods in the optical regime [74].

Unlike pure quantum effects, the FRs can be treated classically and they clearly show themselves in the experiments investigating the linear (first harmonic) response. A long lifetime plasmon mode (quadrupoles, dark mode) can behave as a quantum object. In Fig. 2.7 (a1), split ring resonator structures which couple to each other are demonstrated [74]. Only one of the ring (dipoles-right) couples with the incoming radiation. The one on the left supports dark quadrupole mode (does not couple with incoming radiation). It has 10 times longer lifetime compared the SRR which supports the dipole one. The Fano resonance dip in Fig 2.7 (a2) in weak coupling regime (red) and splitting in strong coupling regime (blue) is observed because of the coupling between the two split ring resonators (SRRs).

The same effect can also be seen in the optical regime, see Fig. 2.7(b1) [75]. The grey nano bar works like a resonator in dipole resonance. The blue bars below the grey nano bar behave as a quadrupole resonator. We identify the absorption dip at the quadrupole blue nanorods' eigenfrequency while the grey nano bar is excited. The Fano dip can also be observed when a substance with a sharp dielectric function (i.e., Quantum emitter) is positioned at the MNP hot spot Fig 2.8.

The principle disadvantage with surface plasmons (SP) is their very short lifetime. This limits various applications such as solar cells [23]. Fano resonances not only display a tranpaency window at the frequency of the longer lifetime object. Fono resonances can also in-

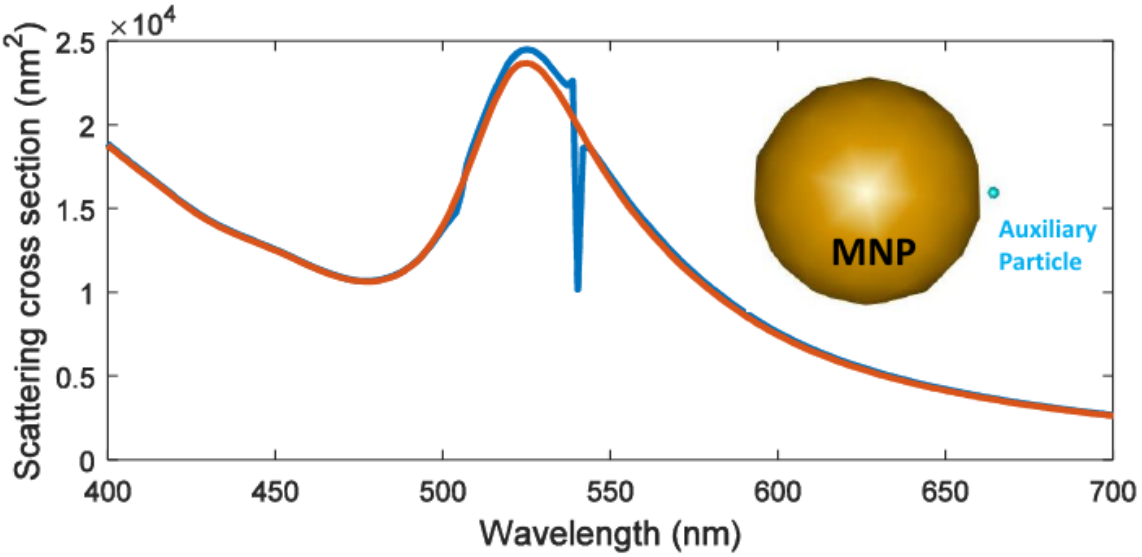

Figure 2.8: Fano dip formation at scattering cross section graph (blue) by auxiliary object (quantum emitter) placed in the hot spot of the gold MNP [19].

crease the effective lifetime of the plasmon excitations [76, 77, 23]. Fano-enhanced plasmon lifetime yields a further accumulation in hot spots. These are called as dark hot resonances. In other words, a dip in the absorption spectrum, enables longer plasmon trapping [29]. The lifetime enhancement enables the operation of spasers (Surface Plasmon Amplification by Stimulated Emission of Radiation).

This phenomenon can also be implemented for achieving further enhancements in the nonlinear systems, i.e., four-wave-mixing (FWM) [27] and SERS [78, 79, 28]. Moreover, Fano resonances can enhance the steady-state of a nonlinear process without increasing the hot spot intensities [80]. This allows the Raman imaging of fragile molecules.

Fano resonances can be utilized for controlling the nonlinear response of via two methods (i) Nonlinearity of metal nanostructures can be enhanced both by localizing the driving (laser) and the converted fields. For instanec, a Raman proess is enhanced 10^8 times, when the hot spot intensity of the driven and converted are each by 10^4. This is utilized in Surface Enhanced Raman (SER) [5], Four wave Mixing (FWM) [7] and Second Harmonic Generation (SHG [6] succesfully. The lifetime enhancement effect of a Fano resonance can further enhance each hot spots by a factor of 10 - 10^2. Thus, the nonlinearity becomes enhanced by a total factor of (10^2 x 10^4)x(10^2 x 10^4) = 10^{12} [21, 22, 23, 24, 25]. As described previous section FRs can contribute the local field enhancement via path interference effects. This ad-

ditional enhancement in the hot spots contributes the enhancement at nonlinear response. (ii) The nonlinear response can be enhanced or suppressed by the FRs via path interference effects without altering the hot spot intensity of the driven mode. This enhancement type (in difference) works in the steady-state. The coupling to an auxiliary object both classical or a quantum can lead path interference effects on the nonlinear response. Moreover, the coupling of the frequency converter with the long life-time mode (dark plasmon) can enhance or suppress the nonlinear processes.

2.5.1 Effect of the coupling strength

The coupling strength between a bright plasmon mode and a quantum object (can also be a dark mode) plays a crucial role in Fano resonances. Weak and strong coupling regimes are defined, e.g., for a system of interacting QD (as an atom-like emitter) and a MNP hot spot, by compering the plasmon-exciton coupling strength (g) and the decay rates of the plasmons (γ_p) and the QE (γ_{eg}). Fano resonances can be observed in the weak coupling regime [81]

$$g < \frac{(\gamma_p - \gamma_{eg})}{4}, \tag{2.8}$$

The Purcell effect, enhancement of the spontaneous emission rate of a quantum emitter near a MNP, can also be observed in the weak coupling regime (see Fig. 2.9)

In the strong coupling regime [81, 82]

$$g > \frac{(\gamma_p - \gamma_{eg})}{4}, \tag{2.9}$$

the two oscillators exchange their energy much faster than the energy leaks away. In this regime, the excitation of the QE is directly transferred to the MNP and the fluorescence is quenched [82].

In an experimental sturdy, one can test the strong coupling regime by examining if two eigenmodes split from those of non-interacting ones due to the coupling. In Fig. 2.10a experimental studies achieved strong coupling conditions with QDs placed in the middle of the silver bowtie antennas made with lithography techniques [83]. For the coupling strength

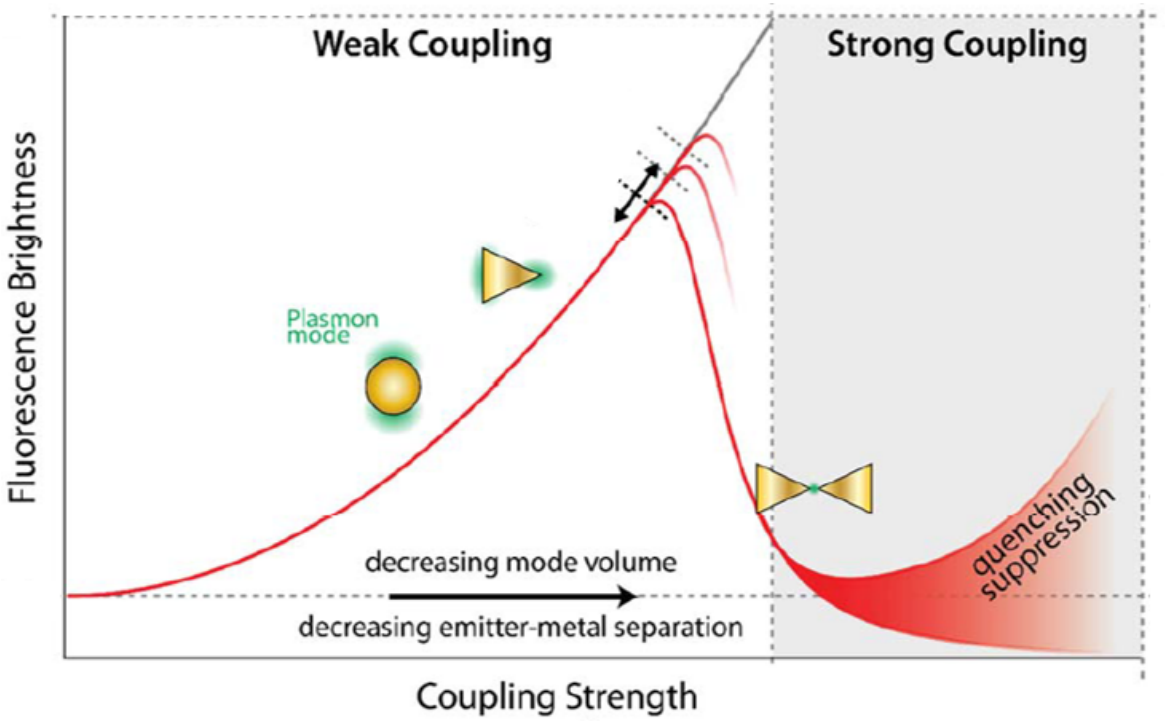

Figure 2.9: Fluorescence brightness of a quantum emitter coupled to a plasmonic nanocavity. As the mode volume of interaction decreases the coupling strength increases results in decreasing the fluorescence rates in strong coupling regime conditions. Figure is adapted from Ref.[82].

150 meV (Fig. 2.10b) of QD to the plasmonic cavity, Rabi splitting was observed at the scattering cross-section signal of the system. Furthermore, coupling strength over 200 meV are reported in Refs. [84, 85].

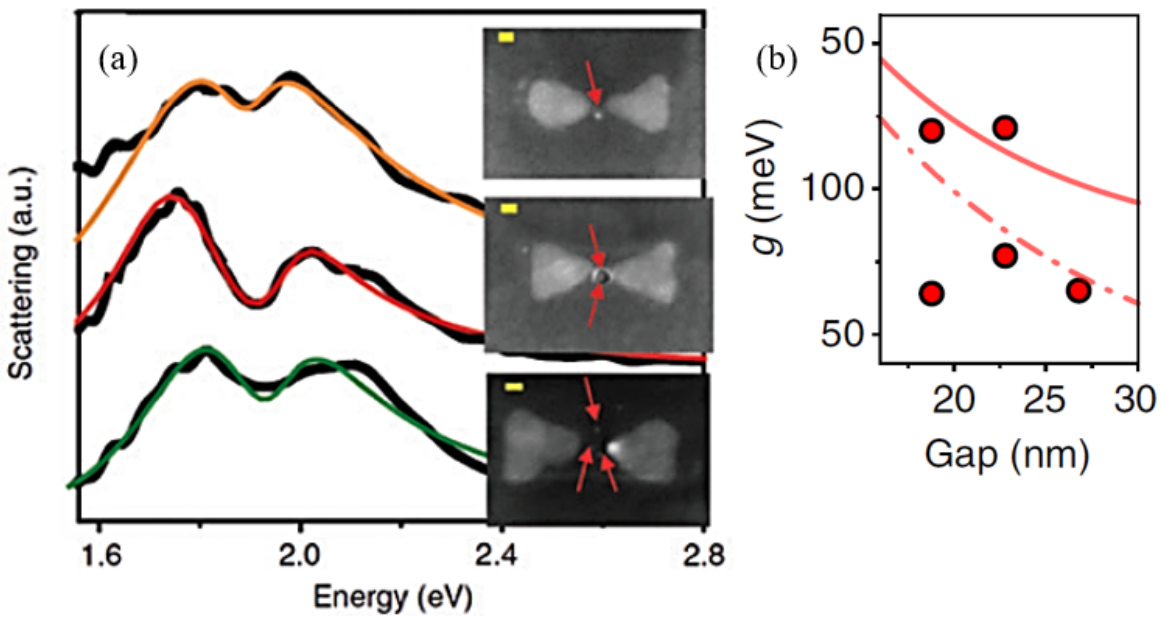

Figure 2.10: a) Experimental demonstrations of the coupling strengths for bowtie antenna and QDs interaction. b) Coupling strengths as a function of the gap size for bowtie antenna [83].

.

3 CONTROLLING THE SECOND HARMONIC SIGNAL VIA LINEAR AND NONLINEAR FANO RESONANCES

Metal nanoparticles (MNPs) can trap incident radiation into nm-sized hot spots as localized surface plasmon (LSP) oscillations. Hot spot intensity (near-field) can be 10^5 times that of the incident field [2, 3] or even higher [4]. Such a localization makes important detection and manipulation technologies possible. For instance, a fluorescent molecule becomes detectable in the vicinity of the hot spot [86, 87], which would not be possible with a weak-intensity incident field. Localization also strengthens the nonlinear properties of molecules positioned in the vicinity of the hot spots. Signal from a Raman-reporter molecule can be enhanced remarkably [5]. Such a great increase in the signal results from the localization of both the incident and the produced (Raman) fields [88] . In this way, surface enhanced Raman scattering (SERS) enables detection of Raman signal even from a single molecule. Second harmonic generation (SHG) also increases orders of magnitude via arranging both the fundamental (ω) and second harmonic (2ω) fields with plasmon resonances [89].

Enhanced hot spot field also makes path interference effects (Fano resonances) possible [65, 90]. In an FR, the weak hybridization is induced by the interaction of the plasmon near field with the QE. An FR can appear when the plasmon mode of the MNP is coupled to an excitation with a longer lifetime (or narrow-band equivalent). For instance, FR can appear in an all-plasmonic system when the excited LSP is coupled to a long lived dark plasmon mode [74, 75].

FRs can control linear and nonlinear properties of MNPs [91, 92, 93, 18]. They can do this in two ways. First, FRs can increase the lifetime of plasmon excitation [76, 77, 25]. In the same incident field strength, an MNP with an FR can accumulate more intense field at the hot spot. These are called as dark-hot resonances [26]. This enhancement in the plasmon lifetime enables the operation of spasers [29, 30], nano-lasers. Dark-hot resonances appear strongest when the incident field is resonant to the transparency window [26]. Even though excitation reaches the transparency (zero) in the steady state, the hot spot becomes more intense for some time due to enhanced plasmon lifetime. Dark-hot resonances are cleverly adapted in enhancing the SERS [78, 79, 28] and FWM [27] signals further. Several orders of magnitude extra enhancement multiplies the enhancement due to localization. For

instance, a double resonance system, where exciting and converted frequencies are tuned to two plasmon resonances [94], can yield a stronger SERS signal. Besides that, when exciting and converted frequencies are aligned with two FRs, then the signal can be enhanced several orders on the top of the double resonance scheme. One can conduct similar results also for the SHG process [89].

Second, Fano resonances can also tune the steady state linear and nonlinear response. Steady-state nonlinear response of SHG [6],THG,FWM [20] and SERS [80] processes. Depending on the choice of the coupled QE's level-spacing (ω_{eg}), nonlinear response can be both enhanced and suppressed. In this Chapter, we study the control of steady-state second harmonic signal by path interferences both (i) in the linear and (ii) nonlinear responses. We use the path interference which boosts the (i) linear response, thus, also second harmonic generation. That is, the first (i) method improves the intensity of driven (first-harmonic -ω) hot spot. The enhanced ω field creates better SH (2ω) field. We also use a (ii) path interference scheme [80], which increases only the nonlinear response without increasing the strength of the driven hot spot field. This technique can be useful when a powerful pulsed laser excites the MNP-QE hybrid device. For instance, experiments using a type of molecule with a very weak SHG response, will require a strong pulsed laser. In the presence of a dark hot resonance or enhancement, this may heat the molecule too much and destroy it. So we can not use the method (i) we presented here. In such a case, it would be very useful to enhance the second harmonic signal without increasing the strength of the driven hot spot field. It is demonstrated that all-plasmonic FRs can suppress SHG [95]. Here, we show that such a suppression is also possible in the presence of a molecule resonant to the second harmonic signal. Unlike previous studies [6, 95], we demonstrate the suppression phenomenon via solving the 3D Maxwell equations exactly. The Lorentzian dielectric function was used for simulating the molecule [3] and demonstration of the suppression. This was predicted by an analytical method [17] previously but hos not been confirmed with 3D solutions. Enhancement of SH signal via a linear Fano resonances has also not been conducted before [96, 19].

We introduce an analytical model basically and check against the results of the model with the exact solutions of 3D Maxwell equations. In particular, we observe the suppression phenomenon via FDTD simulations using realistic functions. We carry out numerical calculations for investigating the FR effects on the SHG signal utilizing the 3D-FDTD (Finite

Difference Time Domain) simulations. We simulate a MNP-QE hybrid structure using experimental dielectric functions. The FDTD method relies on the discretization of Maxwell's equations in a spatial (typically inside a rectilinear cartesian grid originally established by Yee in 1966 [97]) and temporal domain. Owing to its simple and explicit approach, FDTD method is widely used in the electromagnetic (EM) simulation of nanostructures [98]. FDTD method can handle nonlinear optics simulations in the time domain. Nonlinear effects can be calculated exactly via implementing nonlinear properties ($\chi^{(2)}$, $\chi^{(3)}$) to the materials or environments.

The organisation of this chapter is: In Section 3.1, we represent a basic analytical model for the coupled MNP-QE nonlinear system. We describe the mechanism for the SHG processes in plasmonic nano-materials. We derive an efficient Hamiltonian for a second harmonic converter MNP coupled with a QE. The equations of motion for the plasmon modes of the MNP and the QE are derived. In Section 3.2, we discuss two different enhancement schemes. In Section 3.2.1, we arranged the resonance frequency (ω_{eg}) of the QE such that it is coupled to the driven plasmon mode, $\hat{a}_1$ in Figure 3.1. This enhances the steady-state intensity of the hot spot, consequently the second harmonic signal, which proportionally depends on the hot spot field. In Section 3.2.2, we couple the QE to the $\hat{a}_2$ mode in which second harmonic oscillations take place. This enhances the second harmonic signal without altering the hot spot field intensity of the driven $\hat{a}_1$ mode. Section 3.3 involves the comparison of analytical results with 3D-FDTD calculations. Section 3.4 contains our conclusions.

3.1 Analytical Model

In this section, we derive the effective Hamiltonian for a plasmonic second harmonic converter coupled to a QE. Hamiltonian contains two possibilities; QE coupled to (i) driven $\hat{a}_1$ mode and to the (ii) high energy plasmon mode $\hat{a}_2$ into which second harmonic oscillations take place. We derive the equations of motion for each case. These equations are the basis on which we discuss how one can gain control over the nonlinear signal with and without modifying the linear response.

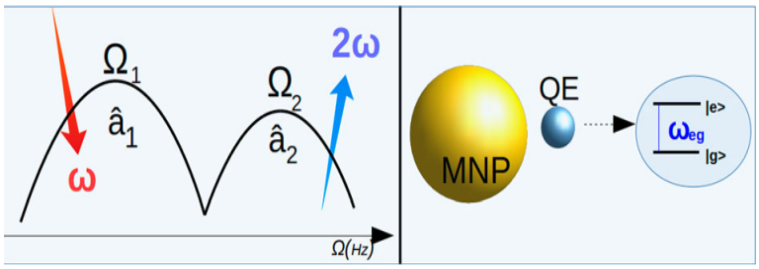

Figure 3.1: (Left). Schematic description of the two plasmon modes, $\hat{a}_1$ and $\hat{a}_2$ involved in the SHG process [100]. Incident field with the frequency of ω excites $\hat{a}_1$ mode. At the hot spot, two ω plasmons combine to form a single $\hat{a}_2$ mode (2ω) plasmon. SHG process takes place in between the two plasmon modes [100] since the overlap integral in Equation (3.1) becomes largest for both ω and 2ω are localized. (Right). A QE of level spacing ω_{eg} can be chosen to couple either (i) the $\hat{a}_1$ mode, Ω_1 or (ii) to the $\hat{a}_2$ mode, Ω_2. Different path interference schemes result in the two nonlinearity control mechanisms, see Figures 3.2 and 3.3.

3.1.1 Hamiltonian

SHG (frequency doubling) process in a plasmonic nanomaterial can be described as follows. When plasmonic structure is illuminated with a powerful incident laser field (ε_L) with the frequency of ω, the plasmon oscillations in the $\hat{a}_1$ mode are excited. Combination of the two plasmons in the $\hat{a}_1$ mode creates a single plasmon in the $\hat{a}_2$ mode [99] oscillating as $e^{-i2\omega t}$. Second harmonic conversion process takes place between plasmons [92, 100, 101, 18] since the overlap integral for the conversion process, Equation (3.1) below, attains a large value.

The interaction hamiltonian for the SHG process, taking place in the can be written as

$$\hat{\mathcal{H}}_{\text{sh}} = \left[\int d^3r \chi^{(2)}(\mathbf{r}) E_2^*(\mathbf{r}) E_1^2(\mathbf{r})\right] \hat{a}_2^\dagger \hat{a}_1 \hat{a}_1 + h.c. \tag{3.1}$$

The integral in the parenthesis, $\chi_2 = \int d^3r \chi^{(2)}(\mathbf{r}) E_2^*(\mathbf{r}) E_1(\mathbf{r})^2$, is the overlap integral [18], where $\chi^{(2)}(\mathbf{r})$ is the second order polarization in dimensions of [ϵ_0/E-field]. $\chi^{(2)}(\mathbf{r})$ is considered as a 3D step function. Here, χ_2 determines the strength of the SHG process, (ii) demonstrates us why second harmonic conversion takes place between plasmon of different frequencies and (iii) gives the selection rules for the SHG process. For instance, an efficient SH conversion cannot be observed in centro-symmetric nanostructures unless the $E_2(\vec{r})$ possesses an even character, e.g., a quadrupole mode. Otherwise, integral vanishes. When a QE

couples to one of the hot spots of the MNP, it strongly interacts with that mode. The weak hybridization the QE creates a two or more absorption/emission paths come into play [73]. Also becomes apparent below, depending on the level spacing (ω_{eg}) of the QE, it is possible to introduce different interference schemes. Hamiltonian of the system can be written as the sum of the energies of the plasmon oscillations (Ω_1, Ω_2), QE (ω_{eg}) the energy transferred by the pump source (ω)

$$\begin{aligned} \hat{\mathcal{H}}_0 &= \hbar\Omega_1\hat{a}_1^\dagger\hat{a}_1 + \hbar\Omega_2\hat{a}_2^\dagger\hat{a}_2 + \hbar\omega_{eg}|e\rangle\langle e|, \\ \hat{\mathcal{H}}_L &= i\hbar(\varepsilon_L\hat{a}_1^\dagger e^{-i\omega t} - h.c.), \end{aligned} \tag{3.2}$$

the SHG process $\hat{\mathcal{H}}_{sh}$ defined in Equation (3.1) and the interaction of the QE with the plasmon-polariton modes $\hat{\mathcal{H}}_{int}$

$$\hat{\mathcal{H}}_{\text{sh}} = \hbar\chi_2(\hat{a}_2^\dagger\hat{a}_1\hat{a}_1 + \hat{a}_1^\dagger\hat{a}_1^\dagger\hat{a}_2), \tag{3.3}$$

$$\hat{\mathcal{H}}_{\text{int}} = \hbar(f_1\hat{a}_1^\dagger + f_2\hat{a}_2^\dagger)|g\rangle\langle e| + h.c. \tag{3.4}$$

Here the parameters f_1 and f_2, in units of frequency, are the coupling strengths of the linear and second harmonic modes ($\hat{a}_2$ of the MNP, respectively. χ_2 is the overlap integral given in Equation (3.1) and $|g>$ ($|e>$) represents the ground (excited) state of the QE.

Dynamics of the system can be obtained using the Heisenberg equations of motion (e.g., $i\hbar\dot{\hat{a}}_i = [\hat{a}_i, \hat{\mathcal{H}}]$). Since we are interested in the intensities only, but do not aim to calculate the correlations, we replace the operators $\hat{a}_i$ and $\hat{\rho}_{ij} = |i\rangle\langle j|$ with complex numbers α_i and ρ_{ij} respectively [102]. The equations of motion can be obtained as

$$\dot{\alpha_1} = -(i\Omega_1 + \gamma_1)\alpha_1 - i2\chi_2\alpha_1^*\alpha_2 - if_1\rho_{ge} + \varepsilon_p e^{-iwt}, \tag{3.5}$$

$$\dot{\alpha_2} = -(i\Omega_2 + \gamma_2)\alpha_2 - i\chi_2\alpha_1^2 - if_2\rho_{ge}, \tag{3.6}$$

$$\dot{\rho}_{ge} = -(i\omega_{eg} + \gamma_{eg})\rho_{ge} + i(f_1\alpha_1 + f_2\alpha_2)(\rho_{ee} - \rho_{gg}), \tag{3.7}$$

$$\dot{\rho}_{ee} = -\gamma_{ee}\rho_{ee} + i\Big\{(f_1\alpha_1^* + f_2\alpha_2^*)\rho_{ge} - c.c\Big\}, \tag{3.8}$$

where $\gamma_{1,2,3}$, γ_p and γ_{ee} represent to the damping rates of crystal modes, the plasmon mode and the quantum emitter, respectively. The conservation of probability $\rho_{ee} + \rho_{gg} = 1$ Here, population inversion $y = \rho_{ee} - \rho_{gg}$ is the off-diagonal decay rate of the QE $\gamma_{eg} = \gamma_{ee}/2$ accompanied (Equations 3.5-3.8).

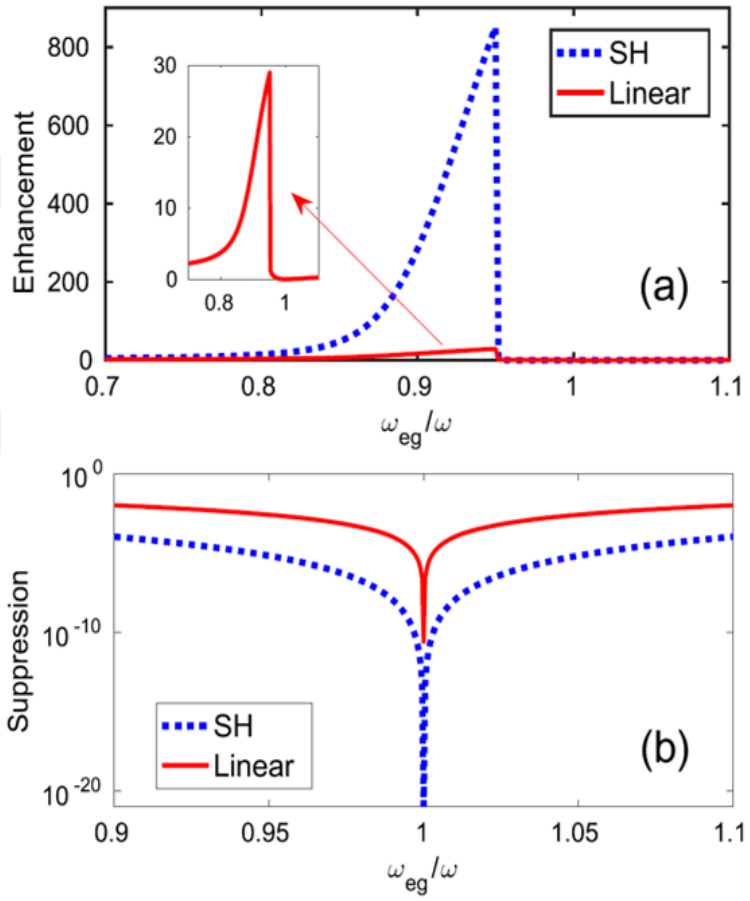

Figure 3.2: Method (i) Fano resonance in the linear response.(a) Enhancement and (b) suppression of the second harmonic (dotted line) and linear (straight line) field intensities for $\Omega_1 = 0.8\omega$ when QE coupled to $\tilde{\alpha_1}$ mode, obtained from time evolution of Equations (3.5)–(3.8). We control the steady-state intensity of driven ($|\alpha_1|^2$) hot spot. (a) The SH intensity is enhanced ∼900 times via the linear enhancement ∼30. (b) The SHG is suppressed $\sim (10^{-10})^2 = 10^{-20}$ times due to linear suppression $\sim 10^{-10}$. We use χ_2 = $10^{-5}\omega$, $f_1 = 0.1\omega, f_2 = 0, \gamma_1 = \gamma_2 = 0.01\omega$ and $\gamma_{eg} = 10^{-5}\omega$.

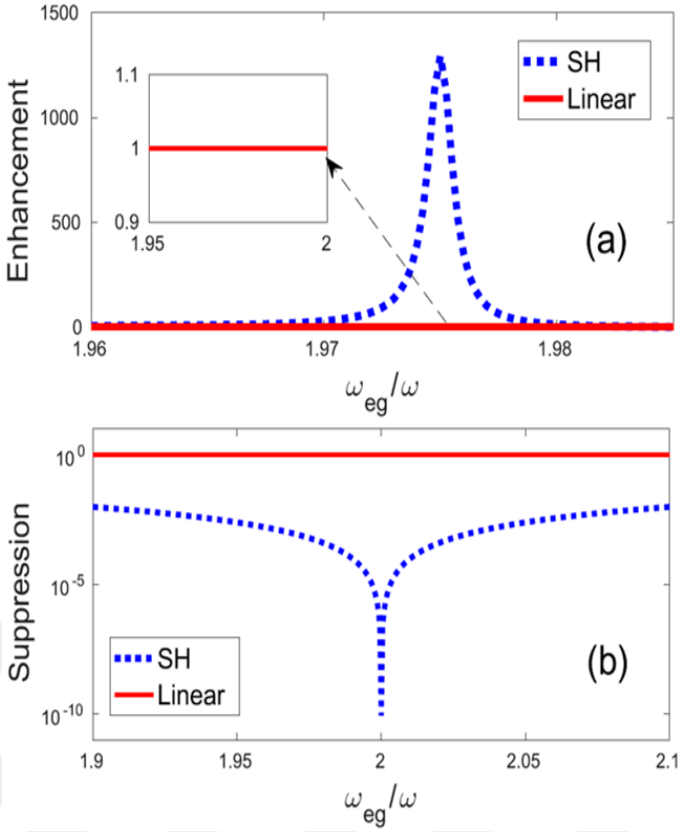

Figure 3.3: Method (ii): Fano resonance in nonlinear response. a) Enhancement and (b) suppression of the second harmonic (dotted line) and linear (straight line) field intensities when QE coupled to α_2 mode, obtained from time evolution of Equations (3.5)–(3.8). The QE is chosen to have no SH response. Both enhancement and suppression factors are calculated with using Equation (3.11). The same parameters are used as in Figure 3.2.

In the steady state, the two plasmon mode amplitudes and the diagonal density matrix elements can be written as

$$\alpha_1(t) = \tilde{\alpha}_1 e^{-i\omega t}, \alpha_2(t) = \tilde{\alpha}_2 e^{-i2\omega t}, \rho_{ee}(t) = \tilde{\rho}_{ee}, \rho_{gg}(t) = \tilde{\rho}_{gg}. \tag{3.9}$$

The off-diagonal density matrix element $\rho_{ge}(t)$ determines the electric polarization of the QE. Its steady-state oscillations take the form $\rho_{ge}(t) = \tilde{\rho}_{ge} e^{-i\omega t}$ and $\rho_{ge}(t) = \tilde{\rho}_{ge} e^{-i2\omega t}$ when QE is coupled to α_1 mode and α_2 mode, respectively. Although, we present our results with the numerical time evolutions of Equations (3.5)–(3.8) in Figures 3.2 and 3.3, we study the steady-state carefully in order to obtain on understanding on different interference schemes.

3.2 Enhancement and Suppression

In this section, we examine the second harmonic response of the plasmonic nano-structure coupled to a QE. The relative enhancement factor (EF) for each mode is defined in the presence and absence of a QE as

$$EF_{\alpha_1} = \frac{|\alpha_1(f_i \neq 0)|^2}{|\alpha_1(f_i = 0)|^2} \tag{3.10}$$

$$EF_{\alpha_2} = \frac{|\alpha_2(f_i \neq 0)|^2}{|\alpha_2(f_i = 0)|^2} \quad i = 1, 2. \tag{3.11}$$

We aim to control the amplitudes of both linear and nonlinear fields. In order to do that, a basic analytical model is used and obtained the steady-state amplitudes for the generated second harmonic plasmons. From a single equation, we demonstrate the origin of enhancement and suppression. We compare two different cases (regimes) for the level spacing of the QE (ω_{eg}). When it is close to the (i) linear and (ii) second harmonic frequency oscillations.We show that in either case enhancement and suppression of the SHG process is possible. In the first case, both enhancement and suppression in the second harmonic field are proportional to the square of the linear field. In the latter case, however, the enhancement can be obtained silently ,i.e., without modifying the hot spot field intensity of the α_1 mode. In Sec. 3.3, we demonstrated the suppression phenomena predicted by our model with 3D FDTD simulations. The observation of SHG in the predicted spectral position is confirmed by the FDTD simulations.

3.2.1 Coupling of quantum emitter (QE) to α_1 mode

Illumination of MNPs by an electromagnetic field with the frequency of ω results in strong field enhancement in the vicinity of the MNPs. By placing QE into these regions, further enhancement in the hot spot field intensities, due to linear FRs, can be obtained. In this part, we show that hot spot field intensity can be enhanced not only in the initial times [26, 23] but also in the steady-state when a QE is coupled to the driven mode (α_1) of the MNP. We also demonstrate the consequences of this process in the nonlinear response.

The enhancement and suppression of the second harmonic field intensity are possible by enhancing the linear response. When a QE is couple to α_1 mode, path interference ef-

fects take place for the linear field intensity. Since we are examining the coupling of QE to the driven mode, interaction strength between QE and second harmonic response can be neglected (e.g., $f_2 \approx 0$) due to far off resonance. Thus, the QE oscillates as $\rho_{ge} = \tilde{\rho}_{ge}e^{-i\omega t}$ in the steady state. Inserting $\rho_{ge} = \tilde{\rho}_{ge}e^{-i\omega t}$ and Equation (3.9) into Equations (3.5)–(3.8), one can find steady-state solution for α_1 and α_2 modes as

$$\alpha_1 = \frac{\epsilon_p}{[i(\Omega_1 - \omega) + \gamma_1] + \frac{f_1^2 y}{[i(\omega_{eg} - \omega) + \gamma_{eg}]}} \tag{3.12}$$

$$\alpha_2 = \frac{-i\chi_2}{[i(\Omega_2 - 2\omega) + \gamma_2]}\alpha_1^2 \tag{3.13}$$

The enhancement of $|\alpha_1|^2$ intensity can be obtained by minimizing the denominator of Equation (3.12). When oscillation frequency of the linear response, Ω_1, is off-resonant with the plasmon resonance ω, the imaginary part of the first term, i.e., can be eliminated by choosing a QE with an appropriate level-spacing ω_{eg}, and/or by tuning the interaction strength (f_1) via adjusting the separation between the MNP and the QE. That is, in the case of choosing level spacing as, $\omega_{eg} \simeq \omega - f_1^2 y/(\Omega_1 - \omega)$, which cancels imaginary part of the first term, about 30 times enhancement can be achieved at the hot spot field intensity (See Fig. 3.2a). Due to quadratic dependence on α_1 in Equation (3.13), the enhancement in the second harmonic generation is approximately square of the linear mode, see Figure 3.2 (a).

Denominator of α_1 in Eq. (3.12) also reveals a suppression phenomenon, i.e., the Fano resonance. When $\omega = \omega_{eg}$ and f_1 is significant, the second term in the denominator of Equation (3.12) becomes $\sim \mathrm{f}_1^2 y/\gamma_{eg}$. When we scale all the frequency terms by the driving field, ω, the γ_{eg}^{-1} term becomes very large.In this case, the term y Eq. (3.12) in the denominator dominates and results in a very small α_1 which produces the seen transparency for the linear field. Thus, a similar transparency appears in the SHG. This is depicted in Figure 3.2 (b).

3.2.2 Coupling QE to α_2 mode

Also, the constructive and destructive interferences of the frequency conversion paths can enhance and suppress the SHG process alone. If the level-spacing of the QE is chosen close to the second harmonic frequency $\omega_{eg} \approx 2\omega$, its interaction with the α_2 mode becomes

stronger compared to α_1 mode as it is highly off-resonant from the driven mode. In addition, the hot spots of each mode can emerge at different spatial positions. By placing QE at the hot spot of α_2 mode, coupling of QE to the driven mode becomes negligible (i.e. $f_1 \approx 0$) due to both effects. One can observe that steady-state solution for the QE is in the form $\hat{\rho}_{eg}(t) = \hat{\rho}_{ge}e^{-i2\omega t}$ where $\hat{\rho}_{eg}$ is a constant in time. Inserting this form into Equation (3.7) and using Equation (3.9), the steady-state amplitude for the plasmons in the α_2 mode can be obtained from Equations (3.5)–(3.8) as

$$\hat{\alpha}_2 = \frac{-i\chi_2}{[i(\Omega_2 - 2\omega) + \gamma_2] + \frac{f_2^2 y}{[i(\omega_{eg} - 2\omega) + \gamma_{eg}]}} \hat{\alpha}_1^2 \tag{3.14}$$

Interpretation of why enhancement and suppression take place in the second harmonic field can be seen by examining the denominator of Equation (3.14). Here, we demonstrate how second harmonic field can be enhanced without any modification in the linear response, $\tilde{\alpha_1}$.

Similar to the previous control methods, the enhancement of $\tilde{\alpha_2}$ intensity can be obtained by minimizing the denominator of Equation (3.14). That is, in the case of choosing level spacing as, $\omega_{eg} \simeq 2\omega - f_2^2 y/(\Omega_2 2\omega)$, which cancels the imaginary part of the first term, second harmonic field intensity can be enhanced about 1500 times. This can be made without changing the linear hot spot intensity, see Figure 3.3 (a). The enhancement factor (EF) in Figure 3.3 (a) is obtained for the choice of $\Omega_2 = 1.6\omega$ and the interaction strength $f_2 = 0.1\omega$. For a high-quality plasmonic nano-structure [103], this factor can be even larger.

The denominator of Equation (3.14) also demonstrates us the possibility of an SHG suppression effect. We examine the denominator of the last term in Equation (3.14). When the choice of the level spacing of a QE close to the second harmonic frequency $\omega_{eg} \approx 2\omega$, the last term becomes f_2^2/γ_{eg}. Typical values for the decay rates of QEs are very small compared to all other frequencies. For example it can be $\gamma_{eg} \sim 10^{-6}\omega$ for quantum dots (QDs) [104]. With a coupling constant of sufficient strength, the f_2^2/γ_{eg} term dominates the denominator of Equation (3.14) and suppression of the second harmonic field emerges, see Figure 3.3 (b). Here, we stress that we do not observe any change in the linear field intensity.

We underline that the results presented in Figures 3.2 and 3.3 are the exact solutions of

Equations (3.5)–(3.8) without any approximation.

We note another important point. For the system parameters, we treat as a sample system, (i) enhancement of the linear response, i.e. α_1, appears rather small, about 30 times. When we compare this with the (ii) nonlinear FR method, SHG enhancement from (ii) appears larger. However, this observation can change dramatically for using a sample system with different parameters. Enhancement via linear FRs, in general, can be expected to be much larger than the nonlinear FRs. Because SHG enhancement with linear FR is the square of the linear response, which can be more than two orders of magnitude in other systems.

3.3 3D FDTD Simulations

Suppression of SHG in an all-plasmonic system is experimentally demonstrated in Ref.[95]. In this experiment a long lived dark mode's utilized for the suppression phenomenon. Ref. [17] analytically demonstrated that a similar suppression phenomenon can be achieved also using quantum objects. As the Boundary Element Method (BEM) Ref. [17] used treats the SHG approximately, the suppression of the SHG via the second method given in Fig. 3.3 could not have been demonstrated. Here, we use self-consistent Maxwell equations treating SHG exactly and demonstrate the presence of the anticipated suppression effect (Fig. 3.3) with 3D-FDTD (Finite Difference Time Domain) method simulations. In FDTD method electric fields and magnetic fields are computed for every points of simulation area in the time domain by solving the Maxwell equations.

The computational region is surrounded perfectly matching layers (PML) in order to truncate the computational geometry. These boundary regions absorb the electromagnetic waves with no reflection back to the calculation area. The Maxwell equations and the boundary conditions for the 3D Cartesian simulation grid are given in the Appendix (Section 3.5).

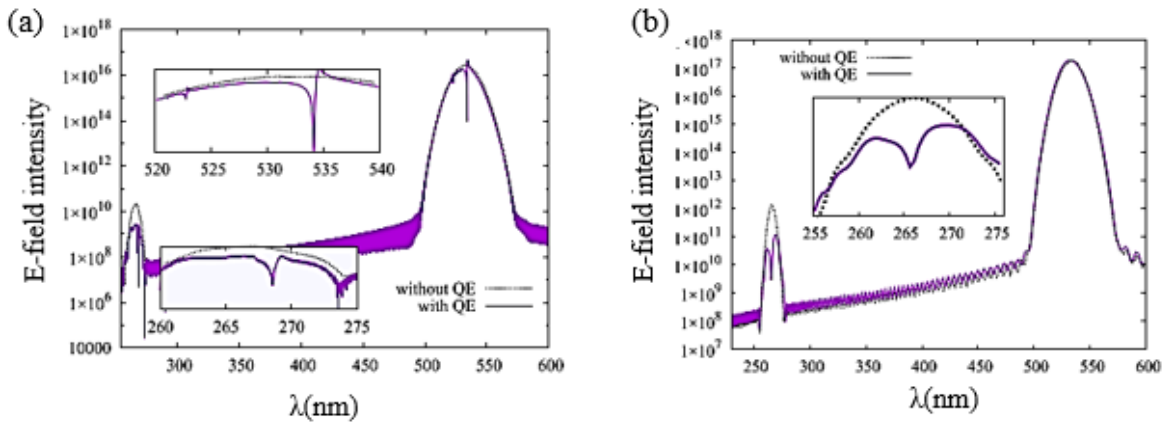

Figure 3.4: FDTD simulations of the second harmonic generation in a coupled MNP-QE system depicted in Fig 3.5. Suppression of SH conversion when QE is coupled to (a) α_1 and (b) α_2 modes of the SH converter MNP. The SHG can be suppressed by utilizing the FRs both in the (a) linear and (b) nonlinear response. Suppression effect when QE is coupled to (a) α_1 and (b) α_2 modes of MNP, obtained from FDTD simulation. (a) Electric field intensity $(V/m)^2$ in the presence (straight line) and absence (dotted line) of QE having a sharp resonance at λ_{QE} = 530 nm. The insets magnify the linear (top) and the second harmonic (bottom) field intensity regions and (b) Electric field intensity $(V/m)^2$ in the presence (straight line) and absence (dotted line) of QE having a sharp resonance at λ_{QE} = 265 nm. The inset magnifies the second harmonic field intensity region.

In Figure 3.4, we compare the predictions of our analytical model for suppression effect with the 3D-FDTD simulation (we used "*Lumerical FDTD: 3D Electromagnetic Simulator*" package program[105]) in which Maxwell's equations can be solved using conventional Yee cell algorithm [97]. We use nano-spheres for the MNP and the QE as in Figure 3.5. Radii of the gold nanoparticle and QE are 35 and 15 nm, respectively. We use the experimental data for the for linear $\chi(\omega)$ and nonlinear $\chi^{(2)}(\omega)$ polarization of gold nanoparticle [106] with $\chi^{(2)}$ nonlinearity[3]. We place an auxiliary QE in the vicinity of the MNP, which has a Lorentzian dielectric function. The Lorentzian peak is centred around 530 nm in Figure 3.4 (a) and 265 nm in Figure 3.4 (b). The excitation wavelength is λ_{exc} = 530 nm with 30 THz bandwidth. The planewave source with the amplitude of the beam is set to 10^6 V/m which has a strong nonlinear response. In Figure 3.4(a) the driven mode (α_1) of the MNP strongly interacts with QE. The QE has a sharp resonance at λ_{QE} =530 nm. The anticipated suppression (Fig. 3.2b) emerges in both modes, see insets of Figure 3.4 (a).

We also study the FDTD simulation of the second control method, Fig. 3.3, i.e., the Fano resonances in the nonlinear response. When a gold-MNP strongly interacts with the QE which has a sharp resonance at λ_{QE} = 265 nm, the suppression in the second harmonic response λ_{SH} emerges without a significant change in the linear response, see Figure 3.4 (b). We wanted to be sure about the origin of the dip which appears at 265 nm in Figure 3.4(b). In order to remove the possibility for the observed dip originating from the absorption induced by QE, we illuminated the sample by a pulse centred at 265 nm and checked if a linear resonance appears. Since we observed the linear with the 265 nm illumination FR, we ensured that dip does not originate from absorption.

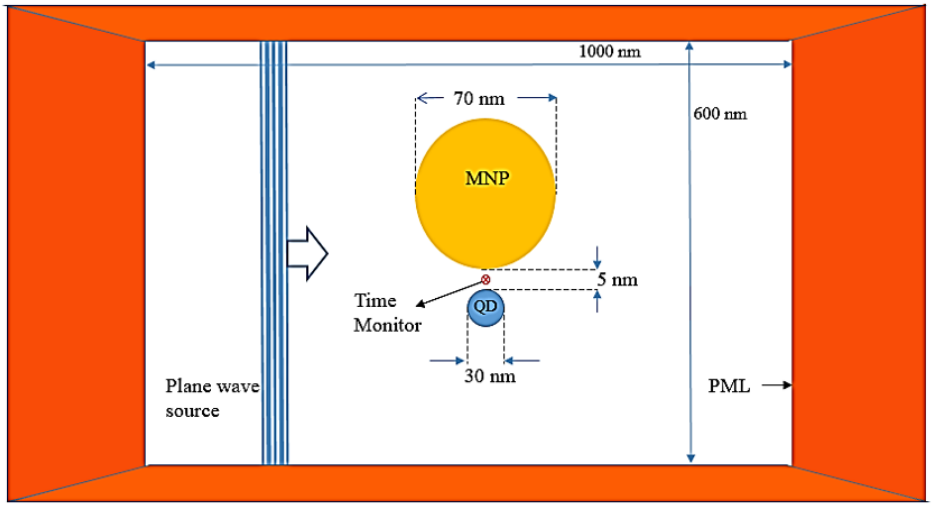

Figure 3.5: Illustration of geometry used in the FDTD simulations. A MNP-QD dimer separated by 5 nm and illuminated with a y-polarized plane-wave source of 30 THz bandwidth. Diameters of the gold MNP and QD are chosen as 70 nm and 30 nm, respectively. We use experimental values for the linear $\chi(\omega)$ and nonlinear $\chi^{(2)}(\omega)$ polarizations of gold MNP. The QD is modelled with a Lorentzian dielectric function [3]. The Lorentzian peak is set to (i) 530 nm snd (ii) 265 nm in simulating the methods in Fig. 3.3 and 3.4, respectively. The perfectly matched layers (PMLs) was used to truncate the computational region.

3.4 Conclusions

We demonstrate that one can gain control over the steady-state second harmonic signal from a plasmonic nano-material via two kinds of FRs. In the first method, linear FR, one can increase the driven (first harmonic) hot spot intensity via an auxilary QE without increasing the pump field. This also increases the second harmonic signal, $P_{2\omega} \sim E_{\omega}^{2}$. The linear Fano resonance method, we develop here, is different than the one widely utilized in the literature [26]. The FRs at Ref. [26] enhances the hot spot intensity by increasing the lifetime of plasmon oscillations [23]. In Ref. [26] enhancement takes place at the same frequency with the auxilary long-lived dark mode. Where as, in our method (i) the steady state enhancement takes place not at the level-spacing of the QE, see Fig. 3.3. In the second method, a nonlinear FR, one can gain control over the second harmonic signal without altering the hot spot field intensity of the driven (first harmonic) mode. Using the exact solutions of Maxwell equations, we also show that the second harmonic signal is suppressed when the QE is tuned to $\omega_{eg} = 2\omega$, as predicted [17]. This phenomenon has also been observed experimentally for all-plasmonic FRs [93, 95]. The comparison shows that analytical model correctly describes the path interference effects.

3.5 Appendix

Maxwell's equations in a source-free, 3D Cartesian grid coordinates are given by

$$\begin{aligned}
\frac{\partial E_x}{\partial t} &= \frac{1}{\epsilon}\Big(\frac{\partial H_z}{\partial y} - \frac{\partial H_y}{\partial z}\Big) & \qquad \frac{\partial H_x}{\partial t} &= \frac{1}{\mu}\Big(\frac{\partial E_y}{\partial z} - \frac{\partial E_z}{\partial y}\Big) \\
\frac{\partial E_y}{\partial t} &= \frac{1}{\epsilon}\Big(\frac{\partial H_x}{\partial z} - \frac{\partial H_z}{\partial x}\Big) & \qquad \frac{\partial H_y}{\partial t} &= \frac{1}{\mu}\Big(\frac{\partial E_z}{\partial x} - \frac{\partial E_x}{\partial z}\Big) \\
\frac{\partial E_z}{\partial t} &= \frac{1}{\epsilon}\Big(\frac{\partial H_y}{\partial x} - \frac{\partial H_x}{\partial y}\Big) & \qquad \frac{\partial H_z}{\partial t} &= \frac{1}{\mu}\Big(\frac{\partial E_x}{\partial y} - \frac{\partial E_y}{\partial x}\Big)
\end{aligned} \tag{3.15}$$

Boundary regions in FDTD method are used to truncate the simulation region by emulating the the free space with Perfectly Matched Layers(PML). The PML was introduced by J. P. B´erenger in 1994 [107]. The B´erenger or split-field perfectly matched layer method is based on field-splitting of Maxwell's equations and selectively choosing different values for the "conductivities" (σ and σ^* are electric and magnetic conductivities of boundary region respectively) in different directions. For 2D simulation (without considering z direction) Maxwell Equations reduce to a set of following three equations [108]

$$\begin{aligned}
\epsilon_0\frac{\partial E_x}{\partial t} + \sigma E_x &= \frac{\partial H_z}{\partial y} \\
\epsilon_0\frac{\partial E_y}{\partial t} + \sigma E_y &= -\frac{\partial H_z}{\partial x} \\
\mu_0\frac{\partial H_z}{\partial t} + \sigma^* H_z &= \frac{\partial E_x}{\partial y} - \frac{\partial E_y}{\partial x}.
\end{aligned} \tag{3.16}$$

Eq. 3.17 is the condition for eliminating the reflections at the boundary region and the Eq. 3.18 is the absorbing boundary condition for PML medium.

$$\frac{\sigma}{\epsilon_0} = \frac{\sigma^*}{\mu_0} \tag{3.17}$$

$$\sigma = \sigma^* = 0 \tag{3.18}$$

4 FANO-CONTROL OF AN "UNLOCALIZED" NONLINEAR PROCESS: SPONTANEOUS PARAMETRIC DOWN CONVERSION

Spontaneous parametric down conversion (SPDC) is a second-order nonlinear process, where an incident beam splits into two lower energy beams labelled as signal and idler [1]. There are many kinds of materials, can be found in nature or synthesized chemically exhibiting nonlinear behaviour. Entangled beam/photon pairs can be generated via down-conversion in various degrees of freedom: entanglement in continuous-variables, polarization, space, time and orbital angular momentum [62]. For quantum optics implementations, generation of entangled beam/photon pairs are essential [37]. Entangled beams/photons are key resources for quantum communication and cryptography [38], quantum computation [39] and quantum information [40]. Splitting high energy photons into two lower ones (PDC) can also be used in solar cell applications by means of reducing the energy losses via harvesting the high energy spectrum [41, 42].

PDC plays an important role at quantum optics but (as mentioned in Chapter 2) it suffers from low conversion rates , i.e., one photon out of 10^8 undergoes conversion [46]. Some recent works [47, 48] report on improvement of the conversion efficiency via changing the geometry/structure of the nonlinear crystals. Some other experimental works employ interaction of the down converting crystal with quantum dots (QDs), as quantum emitters (QEs). QDs, embedded into photonic crystal structures [109] and into a nonlinear down-converting crystal, resonant with the down-converted mode [110, 23], are shown to enhance the parametric-down conversion process. Some more recent works utilize the plasmonic localization effect of metal nanoparticles. For instance, recent theoretical studies [60, 61] envision a 5 orders of magnitude enhancement in PDC efficiency when plasmonic nanostructures are embedded into nonlinear crystals. These results make one draw a conclusion that: plasmonic nanoparticles, localizing (concentrating) the field into hot spots (in the crystal medium), can help nonlinearity. Experiments on the integration of plasmonic nanostructures into nonlinear devices, such as fiber glasses [111] and photonic crystals [112, 113] also report enhanced nonlinear response, e.g., on the Raman conversion process. A second harmonic generating cavity, embedded with plasmonic nanostructures, is also experimentally

demonstrated to yield enhanced sum-frequency generation [114, 115, 116, 117].

Fano-resonances in "local" nonlinear effect, where the nonlinear conversion takes place at the hot spot, have been studied extensively in the literature [8, 10, 9]. In the conventional nonlinear frequancy converters mentioned above, however, the frequency conversion takes place along the whole body of a crystal. That is conversion process in "unlocalized", e.g., not originates from a nanoparticle nor a single nonlinear molecule. The Fano-control of such "nonlocalized" nonlinear processes is completely different than the localized ones studied in the literature [89]. The interference scheme is different which offers enhancements with small coupling strengths. Here, we work on the Fano-control of unlocalized nonlinear processes.

In this chapter, we study the nonlinear response of a down-converting crystal whose surface is decorated with MNP-QE dimers, see Fig. 4.1(a). MNPs serve as interaction centers [44, 45, 46]. They make the unlocalized down converted field concentrate into their hot posts by interacting strongly with the evanescent field [44, 45, 46]. The QEs, placed at the hot spots, create Fano resonances—path interference effects. Thus, by tuning the level spacing (ω_{eg}) of the QE via an applied voltage [53, 54] one can control the path interference effects. We show that such a setup not only can enhance the down-conversion intensity by 2 orders of magnitude, but also can suppress the the conversion down to several orders of magnitude. It should be emphasized that, this enhancement comes as a further multiplication factor on top of the MNP hot spot enhancement, e.g., on top of the enhancements in [80, 94, 109, 110]

The nondegenerate down-converting system (of ω fundamental, $\omega_2 = 0.3\omega$ signal and $\omega_3 = 0.7\omega$ idler frequencies) which we investigate offers the following features. (i) The nonlinear signal $\omega_2 = 0.3\omega$ can be enhanced 2 orders without enhancing the linear (fundamental) field. So, one can enhance ω_2 intensity further without breaking the operation temperature limit of the nonlinear crystal. Other methods, utilizing the local field enhancement [8, 9, 10], can not do that. (ii) The presented control scheme can be employed together with the local field enhancement schemes. (iii) The nonlinear signal ω_2 can be enhanced without enhancing the ω_3 idler intensity, and vice versa. (iv) One can suppress the nonlinear conversion at a specific frequency, e.g., ω_3, see Fig. 4.3(inset) (v) More importantly, one can perform these operations via tuning the voltage applied on the quantum dots or color-centers [53, 54] sitting on the crystal surface. Controlled positioning of dimers [65] can also work in the

favor of cooperative operation of path interferences from many dimer. We treat the system with a basic analytical model which has proven its compliance [89]. Ref. [89], the first study on Fano-control of unlocalized nonlinear processes, shows that the analytical model we use here succesfully predicts the results obtained from the exact solutions of 3D Maxwell equations. More explicitly; Ref. [89] presents an almost one-to-one match between the analytical model and exact solutions of the second harmonic process. The PDC process, however, is not implemented in conventional Maxwell simulations (none of FEM, FDTD, BEM). So we cannot perform 3D simulations for PDC process and content ourselves with the analytical model.

This chapter is organized as follows. In Sec. 4.1, we introduce the setup for enhancing the PDC process and we describe the physics for PDC taking place in a nonlinear crystal where MNP-QD dimers are decorated on the crystal surface. We describe the hamiltonian, derive equations of motion and obtain steady-state amplitudes for the plasmon fields. In Sec. 4.2, we present the parameter sets where 2 orders enhancement, multiplying the localization enhancement, can be achieved. We observe that, small coupling factors can be sufficient. Sec. 4.3 contains our conclusions.

4.1 Model

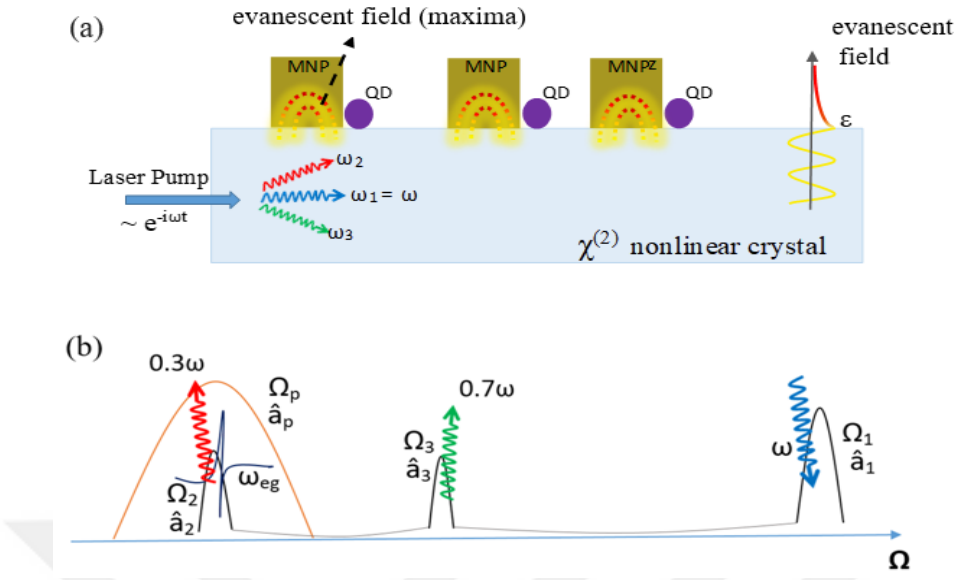

Figure 4.1: (a) A nonlinear crystal performs down conversion process. Metal nanoparticle (MNP)-quantum dot (QD) dimers are decorated onto the crystal surface for controlling the conversion efficiency. The MNPs behave as interaction centers. They localize the generated $\omega_2 = 0.3\omega$ field into the hot spots via coupling strongly to the evanescent waves [116–120]. The quantum emitters (QEs), located at the hot spots, interact with the localized field (that is indirectly with the ω_2 field) strongly and introduce path interference effects. This controls the amplitude α_2 of the $\omega_2 = 0.3\omega$ field. (b) Cavity modes of the nonlinear crystal $\Omega_{1,2,3}$ support the pumped, $\omega_1 = \omega$, and the down converted $\omega_2 = 0.3\omega$, $\omega_3 = 0.7\omega$ oscillations. Down-converted $\omega_2 = 0.3\omega$ photons interact with the MNP-QE hybrid structures. Ω_p is the resonance of the MNP's plasmon mode. Other, possible, modes not involved in the DC process are not depicted. Polarization of the pump $\propto \varepsilon e^{-i\omega t}$ field, determining also the polarization of the down-converted field, is chosen along the dimer axis.(In an actual setup, QDs are placed behind the MNPs.)

A laser of frequency ω pumps the Ω_1 cavity mode of the nonlinear crystal, see Fig. 4.1. The ω oscillations in the Ω_1 cavity mode, $\sim e^{-i\omega t}$, are down-converted into $\omega_2 = 0.3\omega$ and $\omega_3 = 0.7\omega$ oscillations in the cavity modes Ω_2 and Ω_3, respectively (see Fig. 4.1b). We make the cavity field $\omega_2 = 0.3\omega$ interact with the MNP's plasmon mode (Ω_p) and introduce path interference in that converted mode. We choose the signal ω_2 and idler ω_3 frequencies well separated. Because we desire to make the MNP interact only with one of the down-converted

modes. We aim to keep things basic in order to understand "from where the interference origins". We examine the change in the amplitude of the down-converted field, $\sim e^{-i\omega_2 t}$, for different coupling parameters, i.e., between Ω_2 cavity mode and the MNP, g, and between the MNP and the QE, f_c, see Fig. 4.2. We define the enhancement factors by comparing the $\omega_2 = 0.3\omega$ down-converted intensity with and without the presence of the MNP-QE dimers.

We introduce a basic analytical model including the damping rates of the three cavity modes, $\gamma_{1,2,3}$, and the one for the MNP plasmon mode γ_p. We use realistic values for the damping rates one can observe in typical experiments. This is similar for coupling strengths g and f_c. Fabrication of the setup in Fig. 4.1 can be achieved by lithography techniques [58] either by depositing the QDs between the periodic metal nanostructure or by fabricating a periodic structure via controlled positioning of such self-assembled dimers [59].

We note that Fig. 4.1 is a 2-dimensional presentation of the setup in the x-y plane. In an actual 3-dimensional configuration, pump polarization is in the z-direction and QEs are placed behind the MNPs. That is, MNP-QE axis would be along the z-direction.

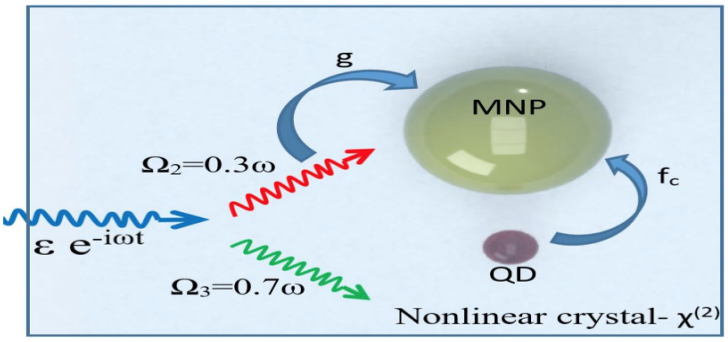

Figure 4.2: A sketch demonstrating the down-conversion and the interaction processes taking place in the nonlinear crystal. The input laser pumps the ω oscillations in the $\hat{a}_1$ (crystal) cavity mode. ω oscillations in the cavity is down-converted into 0.3ω (Ω_2 mode) and 0.7ω (Ω_3 mode) oscillations in the crystal. The 0.3ω oscillations couple (strength g) with the MNP whose plasmon mode (Ω_p) is around 0.3ω. A quantum dot (QD), at the hot spot of the MNP, couples to the plasmon oscillations, at the frequency of 0.3ω. Direct coupling of the QD to the Ω_2 mode, 0.3ω field, is small compared to its coupling to 0.3ω oscillations over the hot spot.

In this section, we first derive an effective Hamiltonian for a down-converting crystal whose surface is decorated MNP-QE hybrid structures. We then obtain the equations of motion for this system and time evolve the equations to obtain the steady-states of the plasmon and down-converted fields.

The hamiltonian for the DC process, taking place in the nonlinear crystal medium, can be written as

$$\hat{\mathcal{H}}_{\rm dc} \;=\; \Big[\int d^3r\, \chi^{(2)}(r) E_1(\mathbf{r}) E_2^*(\mathbf{r}) E_3^*(\mathbf{r})\Big] \hat{a}_3^\dagger \hat{a}_2^\dagger\, \hat{a}_1 + h.c. \tag{4.1}$$

where $E_1^*(\mathbf{r})$, ($E_2(\mathbf{r})$, $E_3(\mathbf{r})$) are the positive (negative) frequency parts of the electric fields. $\hat{a}_j^\dagger$ ($\hat{a}_j$) is the creation (annihilation) operator of the j-th mode. $\chi_2 = \int d^3r\, \chi^{(2)}(r) E_1(\mathbf{r}) E_2^*(\mathbf{r}) E_3^*(\mathbf{r})$ is an overlap integral, which determines the strength of the down conversion process. Here, $\chi^{(2)}(r)$ is a 3D step function which vanishes outside the crystal body.

The total hamiltonian of the system can be written as the terms due to crystal oscillations, pump field, down conversion and interaction

$$\hat{\mathcal{H}}_{\rm total} \;=\; \hat{\mathcal{H}}_0 + \hat{\mathcal{H}}_L + \hat{\mathcal{H}}_{\rm dc} + \hat{\mathcal{H}}_{\rm int} \tag{4.2}$$

The hamiltonian for the crystal oscillations (Eqn. 4.3) contains the pumped (Ω_1) and the down converted (Ω_2 and Ω_3) crystal fields, energy of the plasmon oscillations (Ω_p) and energy of the two-level QE (ω_{eg}). Here $|g\rangle$ ($|e\rangle$) is the ground (excited) state of the QE.

$$\hat{\mathcal{H}}_0 \;=\; \sum_{i=1}^{3} \hbar\Omega_i \hat{a}_i^\dagger \hat{a}_i + \hbar\Omega_p \hat{a}_p^\dagger \hat{a}_p, + \hbar\omega_{eg} |e\rangle\langle e|. \tag{4.3}$$

energy transferred by the laser source is ($\varepsilon e^{-i\omega t}$)

$$\hat{\mathcal{H}}_{\rm L} \;=\; i\hbar(\varepsilon \hat{a}_1^\dagger e^{-i\omega t} - \textit{h.c.}). \tag{4.4}$$

The interaction hamiltonian

$$\hat{\mathcal{H}}_{\rm int} \;=\; \hbar f_c(\hat{a}_p^\dagger |g\rangle\langle e| + |e\rangle\langle g| \hat{a}_p) + \hbar g(\hat{a}_p^\dagger \hat{a}_2 + \hat{a}_2^\dagger \hat{a}_p). \tag{4.5}$$

$\hat{\mathcal{H}}_{\rm int}$ includes the interactions between the down-converted field and the plasmon mode, g, and the interaction between the MNP (plasmon mode) and the QE, f_c. The parameters for the interaction strengths depend on the positions of the particles relative to each other and the spatial overlaps of the cavity and plasmon modes and the overlap of the QE with the hot spots of the MNP. After inserting the overlap integral χ_2 the down conversion process $\hat{H}_{\rm dc}$ can be written as

$$\hat{\mathcal{H}}_{\rm dc} = \hbar\chi_2(\hat{a}_1^\dagger\hat{a}_2\hat{a}_3 + \hat{a}_2^\dagger\hat{a}_3^\dagger\hat{a}_1). \tag{4.6}$$

We use Heisenberg equations of motion (e.g. $i\hbar\dot{\hat{a}}_i = [\hat{a}_i, \hat{\mathcal{H}}_{\rm total}]$) to obtain the dynamics of the system as

$$\dot{\hat{a}}_1 = -(i\Omega_1 + \gamma_1)\hat{a}_1 - i\chi_2\hat{a}_2\hat{a}_3 + \varepsilon e^{-iwt}, \tag{4.7}$$

$$\dot{\hat{a}}_2 = -(i\Omega_2 + \gamma_2)\hat{a}_2 - i\chi_2\hat{a}_1\hat{a}_3^* - ig\alpha_p, \tag{4.8}$$

$$\dot{\hat{a}}_3 = -(i\Omega_3 + \gamma_3)\hat{a}_3 - i\chi_2\hat{a}_1\hat{a}_2^*, \tag{4.9}$$

$$\dot{\hat{a}}_p = -(i\Omega_p + \gamma_p)\hat{a}_p - ig\hat{a}_2 - if_c|g\rangle\langle e|. \tag{4.10}$$

As we are interested in the intensities only, but do not aim to calculate the correlations, we replace the operators $\hat{a}_i$ and $\hat{\rho}_{ij} = |i\rangle\langle j|$ with complex (c-) numbers α_i and ρ_{ij} respectively [102]. So, equations of motion can be obtained as

$$\dot{\alpha_1} = -(i\Omega_1 + \gamma_1)\alpha_1 - i\chi_2\alpha_2\alpha_3 + \varepsilon e^{-iwt}, \tag{4.11}$$

$$\dot{\alpha_2} = -(i\Omega_2 + \gamma_2)\alpha_2 - i\chi_2\alpha_1\alpha_3^* - ig\alpha_p, \tag{4.12}$$

$$\dot{\alpha_3} = -(i\Omega_3 + \gamma_3)\alpha_3 - i\chi_2\alpha_1\alpha_2^*, \tag{4.13}$$

$$\dot{\alpha}_p = -(i\Omega_p + \gamma_p)\alpha_p - ig\alpha_2 - if_c\rho_{ge}, \tag{4.14}$$

$$\dot{\rho}_{ge} = -(i\omega_{eg} + \gamma_{eg})\rho_{ge} + if_c\alpha_p(\rho_{ee} - \rho_{gg}), \tag{4.15}$$

$$\dot{\rho}_{ee} = -\gamma_{ee}\rho_{ee} + i(f_c\rho_{ge}\alpha_p^* - c.c), \tag{4.16}$$

where $\gamma_{1,2,3}$, γ_p and γ_{ee} are the damping rates of crystal modes, the plasmon mode and the quantum emitter, respectively. There exists also a constraint for the conservation of probability, i.e., $\rho_{ee} + \rho_{gg} = 1$. $\gamma_{eg} = \gamma_{ee}/2$ is the off-diagonal decay rate for a single QE.

For obtaining steady state amplitudes of the crystal and the plasmon modes we use the steady state solutions $\alpha_1 = \tilde{\alpha_1}e^{-i\omega t}$, $\alpha_2 = \tilde{\alpha_2}e^{-i\omega_2 t}$, $\alpha_p = \tilde{\alpha_p}e^{-i\omega_2 t}$, $\rho_{eg}(t) = \tilde{\rho}_{eg}e^{-i\omega_2 t}$, $\rho_{ee,gg} = \tilde{\rho}_{ee,gg}$ and $\alpha_3 = \tilde{\alpha_3}e^{-i\omega_3 t}$ inserted into Eqs. (4.11-4.16) and we obtain the steady state equations for the amplitudes as

$$
\begin{aligned}
0 &= -[i(\Omega_1 - \omega) + \gamma_1]\tilde{\alpha}_1 - i\chi_2\tilde{\alpha}_2\tilde{\alpha}_3 + \varepsilon, && (4.17)\\
0 &= -[i(\Omega_2 - \omega_2) + \gamma_2]\tilde{\alpha}_2 - i\chi_2\tilde{\alpha}_1\tilde{\alpha}_3^* - ig\tilde{\alpha}_p, && (4.18)\\
0 &= -[i(\Omega_3 - \omega_3) + \gamma_3]\tilde{\alpha}_3 - i\chi_2\tilde{\alpha}_1\tilde{\alpha}_2^*, && (4.19)\\
0 &= -[i(\Omega_p - \omega_2) + \gamma_p]\tilde{\alpha}_p - ig\tilde{\alpha}_2 - if_c\tilde{\rho}_{ge}, && (4.20)\\
0 &= -[i(\omega_{eg} - \omega_2) + \gamma_{eg}]\tilde{\rho}_{ge} + if_c\tilde{\alpha}_p(\tilde{\rho}_{ee} - \tilde{\rho}_{gg}), && (4.21)\\
0 &= -\gamma_{ee}\tilde{\rho}_{ee} + i(f_c\tilde{\rho}_{ge}\tilde{\alpha}_p^* - c.c). && (4.22)
\end{aligned}
$$

We kindly remind that the frequencies for the signal and idler frequencies $\omega_2 = 0.3\omega$ and $\omega_3 = 0.7\omega$.

As the SHG is an up-conversion process, Ref. [31] is able to obtain an analytical expression for the second harmonic converted field. We place the result obtained in Ref. [31] into the Appendix section (Sec. 4.4) at the end of this chapter. We also provide a brief description for the take place of the path interference for the SHG process in Sec. 3.2. In Ref [31], the analytical expressions in are used to anticipate the presence of the enhancement and the suppression phenomena and they match very well with the 3D-FDTD demonstrations. Unfortunately, here we can not obtain such a simple expression for the down conversion process. Therefore, we cannot demonstrate explicitly how path interference, i.e., cancellations, emerge in the DC process. Nevertheless, one can obtain on insight examining the ones for the SHG in Sec. 3.2.

We simply carry out the time evolution the differential equations, Eqs. (4.17)-(4.22), to obtain the steady state amplitudes.

4.2 Results

In this section, we present the analytical results for the setup depicted in Fig. 4.1 we query if Fano-control of an unlocalized PDC process is possible. We calculate the enhancement of the "signal" intensity $|\alpha_2|^2$ both (i) when surface is decorated with MNPs only and (ii) when surface is decorated with MNP-QE dimers. We anticipate the situation for different parameter sets of interaction strengths g and f_c. As a visualization of comparison (i.e., enhancement factors) we present Table 4.1.

The interaction strength between QE and MNP (f_c) depends on the relative positioning of them. Additionally, size and shape of particles and the overlap of resonance frequencies of MNP with QD cavity modes determine the strength of the interaction. Therefore, coupling strengths can be controlled (not continuously) by setting an appropriate system design, i.e, by arranging MNP sizes and the position of the quantum emitter (QE).

We scale the frequencies with ω, the frequency of the laser pumping the α_1 crystal mode. As the noble metals have resonances in the visible spectrum the frequency of the down-converted signal beam $\alpha_2 = 0.3\omega$ is chosen in the visible spectrum also.

Quantum dot's level spacing (ω_{eg}) can be altered substantially via its size and type. Moreover, ω_{eg} cen be continuously tuned via an applied voltage on the crystal surface. Such a fine-tuning, as becomes apparent in the depicted results, is crucial for achieving Fano resonances. better tuning opportunities are available for defects in 2D materials, which can equally be exploited in the setup Fig. 4.1.

We can illuminate the corresponding physical parameters as follows. By choosing the driving laser frequency as ω ($\omega = 1000$ THz, $\lambda_d = 300$ nm) the energies of coupling strengths f_c and g are tens of meVs (at maximum enhancement: $g = 0.01\omega$ corresponds to 12 meV and $f_c = 0.0025\omega$ corresponds 4 meV) which indicates that the interaction stays in the weak coupling regime which is experimentally more applicable. Since we are at the weak coupling regime, path interference effects-Fano resonances could be seen easier compared to the local schemes.

4.2.1 Definition of Enhancement Factor

As we have a large number of parameters, e.g., ω_{eg}, g, f_c, three different amplitudes $\alpha_{2,3,p}$ to investigate, and three different setup (bare crystal, crystal + MNP, crystal + MNP +QE); we need to categorize the enhancement factors as in Table 4.1. As the principle aim of this work, we can define the down conversion enhancement in the signal (α_2) as

$$\mathrm{EF}_{\alpha_2} = \frac{|\alpha_2(\mathrm{f_c} \neq 0, \mathrm{g} \neq 0)|^2}{|\alpha_2(\mathrm{f_c} = 0, \mathrm{g} = 0)|^2}, \tag{4.23}$$

which compares the number of generated plasmons, $|\alpha_2|^2$, via the MNP-QD dimers with one for a bare crystal. More explicitly, EF is the ratio of the down converted intensities in the presence ($f_c \neq 0, g \neq 0$) and absence ($f_c = 0, g = 0$) of the MNP-QE hybrid structure. We time evolve Eqs (4.17-4.22) and obtain steady state EF, given in Eq.(4.23). We investigate the effect of the MNP-QE dimers on the output signal α_2, idler α_3 and plasmon field α_p. The photon intensities measured in the far-field are proportional to the plasmon intensities $|\alpha_{2,3}|^2$. Because the far-field are generated by plasmons via radiation reaction (simply the oscillating changes).

Table 4.1: Definitions of Enhancement Factors for different signals and configurations.

EF α_2	$\frac{\lvert\alpha_2(f_c{\neq}0,g{\neq}0)\rvert^2}{\lvert\alpha_2(f_c{=}0,g{=}0)\rvert^2}$	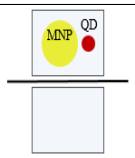	MNP and QD on the surface vs. Bare crystal
EFα_{2QD}	$\frac{\lvert\alpha_2(f_c{\neq}0)\rvert^2}{\lvert\alpha_2(f_c{=}0)\rvert^2}$	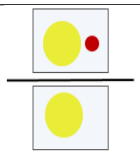	MNP and QD on the surface vs. MNP
EFα_{2MNP}	$\frac{\lvert\alpha_2(g{\neq}0)\rvert^2}{\lvert\alpha_2(g{=}0)\rvert^2}$	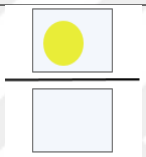	MNP on the surface vs. Bare crystal
EFα_p	$\frac{\lvert\alpha_2(f_c{\neq}0,g{\neq}0)\rvert^2}{\lvert\alpha_2(f_c{=}0,g{\neq}0)\rvert^2}$	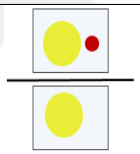	MNP and QD on the surface vs. MNP
EFα_{pMNP}	$\frac{\lvert\alpha_p g{\neq}0)\rvert^2}{\lvert\alpha_p(g{=}0)\rvert^2}$	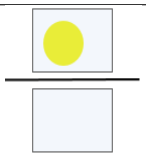	MNP on the surface vs. Bare crystal

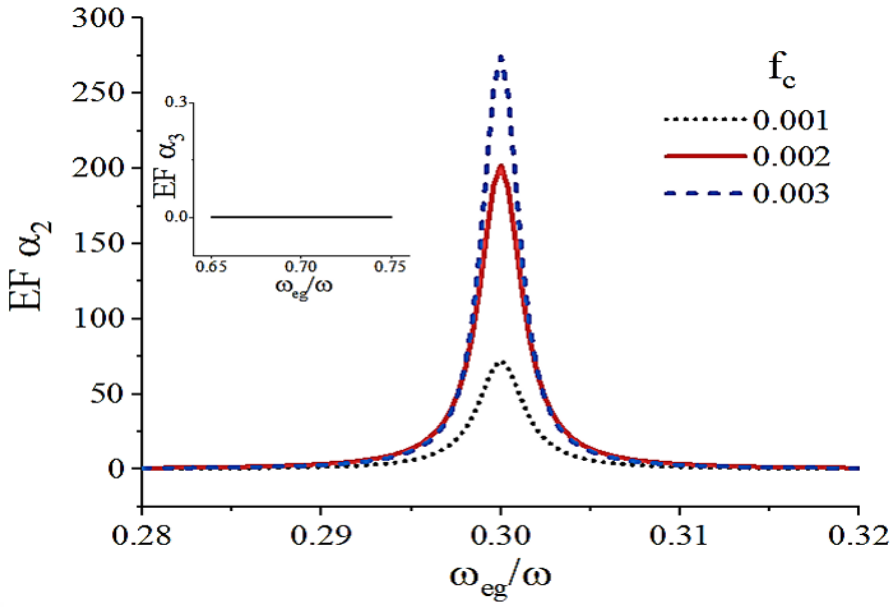

Figure 4.3: Enhancement factor (EF) of the down converted 0.3ω signal intensity (a) versus QE's level-spacing ω_{eg} calculated for different MNP-QE interaction strengths f_c. We set $g = 0.01\omega$ for the coupling of the MNP to the α_2 crystal field. α_2 supports the 0.3ω oscillations. EF plots the $|\alpha_2|^2$ intensity in the presence of MNP-QE dimers compared to the conversion in a bare crystal. Inset shows the EF for the down converted 0.7ω ($|\alpha_3|^2$) signal intensity.

In Fig. 4.3 we present the EF for the down converted α_2 signal intensity with respect to the resonance frequency of QE using Eq. 4.23 for different MNP-QE coupling strength f_c. Fig. 4.3 shows that achieve 300 times enhancement at EF is achieved via path interference effects in the presence of the MNP-QD dimers. The interaction strength between the MNP and the QE, f_c, is set to a value of 0.003ω which is in the weak coupling regime. Fano-control of local nonlinear processes requires f_c $\sim$0.1 ω coupling strengths for achieving similar EFs [80, 31].

All parameters are scaled with ω, the frequency of the laser pumping the α_1 crystal mode. We employ $g = 0.01\omega$, $\Omega_1 = \omega$, $\Omega_2 = 0.3\omega$, $\Omega_3 = 0.7\omega$, $\Omega_p = 0.3\omega$, $\gamma_1 = \gamma_2 = \gamma_3 = 5 \times 10^{-4}\omega$, $\gamma_p = 0.1\omega$ and $\gamma_{eg} = 10^{-5}\omega$. We consider a small second order nonlinear (overlap) susceptibility $\chi_2 = 2 \times 10^{-9}\omega$.

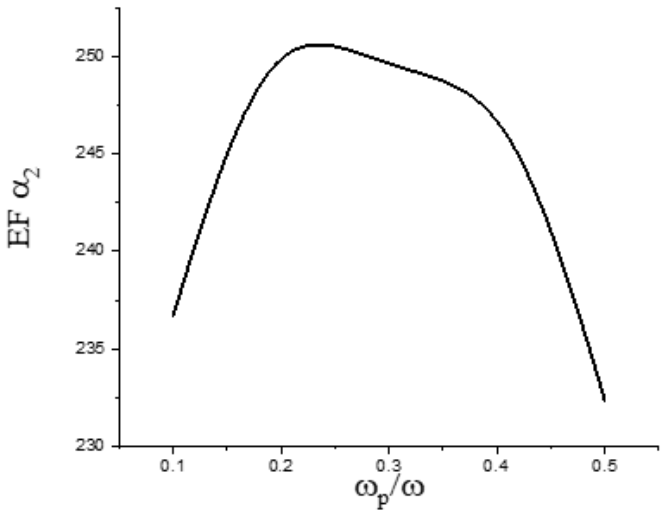

Figure 4.4: Enhancement factor (EF) α_2 (system with MNP-QD structures-Table.1) versus MNP plasmon frequency ω_p calculated for different $g = 0.01\omega$ for the coupling of the MNP to the α_2 nonlinear crystal modes.

In Fig. 4.4 plots the EF α_2 signal with respect to the resonance frequency of the MNP resonance ω_p. It indicates that the enhancement can be achieved in a wide spectrum of the MNP resonance. We note that the MNP resonance frequency depends on the type of material, size and shape of the MNP which can be changed.

We also examine if there appears an enhancement of the signal $|\alpha_2|^2$ when we use only MNPs. Fig. 4.5 shows that presence of MNPs alone merely destroys the $|\alpha_2|^2$ conversion. Nevertheless, the presence of MNPs in a nonlinear crystal can enhance the conversion via localization effect. Our model cannot treat the localization effect.

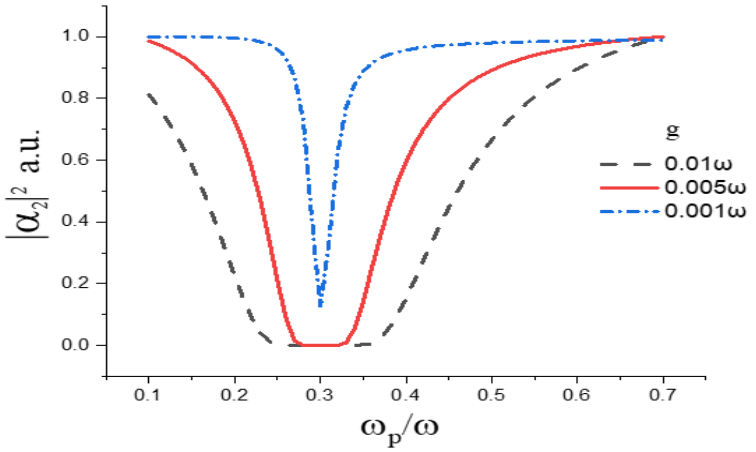

Figure 4.5: Down converted α_2 signal intensity versus MNP plasmon frequency ω_p at the system with only MNPs on the nonlinear crystal.

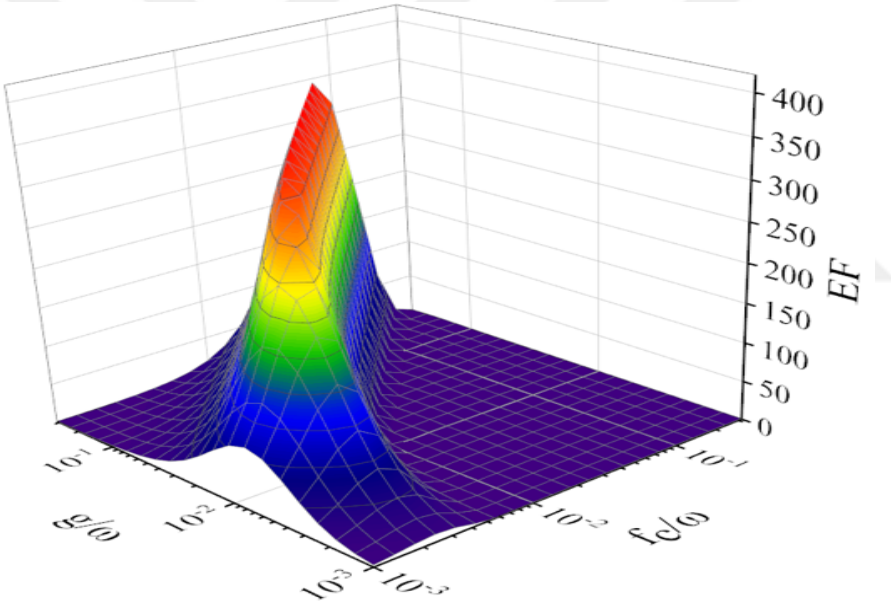

Figure 4.6: Enhancement of the down converted field$|\alpha|^2$ for different values of coupling strengths g and f_c, see Fig. 4.2. EF, at fixed $\omega_{eg} = 0.3\omega$, calculated for different f_c and g couplings. There appears 300 to 400 fold EFs, crudely, for the ratios $f_c/g \sim 1/4$. Other parameters we use are $\Omega_1 = \omega$, $\Omega_2 = 0.3\omega$, $\Omega_3 = 0.7\omega$, $\Omega_p = 0.3\omega$, $\gamma_1 = \gamma_2 = \gamma_3 = 5 \times 10^{-4}\omega$, $\gamma_p = 0.1\ \omega$, $\gamma_{eg} = 10^{-5}\ \omega$ and $\chi_2 = 2 \times 10^{-9}\ \omega$.

Fig. 4.6 demonstrates how the interaction strengths between the MNP and the QE (f_c) and between the MNP plasmon field and the down-converted α_2 field (g) affect the enhancement factor for a fixed QE level spacing ($\omega_{eg} = 0.3\omega$). We observe that enhancement takes

place at a certain ratio of f_c/g. for $f_c < g$. We can crudely determine this ratio as $f_c/g \sim 1/4$, where enhancement of the $|\alpha_2|^2$ down converted intensity appears. When the f_c value gets closer to the g and $f_c \geq g$, enhancement factor (EF) decreases. Around $f_c \geq$, a change in the coupling regime is possible to occur. This actually can be inferred from Fig. 4.7. At $f_c \geq g$ ($f_c = 0.0025\omega$, $g = 0.001\omega$) a Rabi splitting "like" behavior occurs and the Fano enhancement at $\omega_{eg} = 0.3\omega$ vanishes.

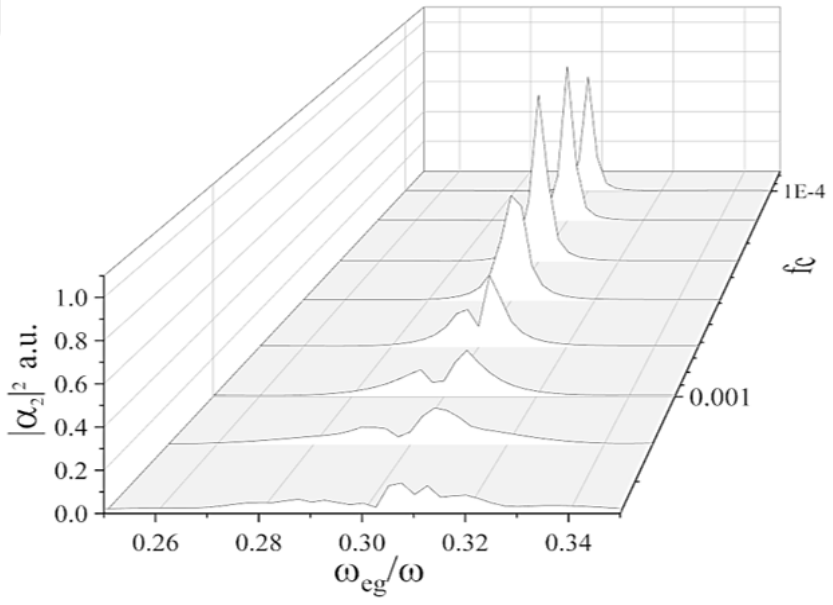

Figure 4.7: The down-converted α_2 signal intensity changes with respect to the MNP-QE interaction strength f_c. For $f_c \geq g$ α_2 signal becomes suppressed at $\omega_{eg} = 0.3\omega$ displaying a Rabi splitting "like" behavior. The parameters are $g = 0.001\omega$, $\gamma_p = 0.001\omega$, $\Omega_1 = \omega$, $\Omega_2 = 0.3\omega$, $\Omega_3 = 0.7\omega$, $\Omega_p = 0.3\omega$, $\gamma_1 = \gamma_2 = \gamma_3 = 5 \times 10^{-4}\ \omega$, $\gamma_{eg} = 10^{-5}\omega$, and $\chi_2 = 2 \times 10^{-9}\ \omega$.

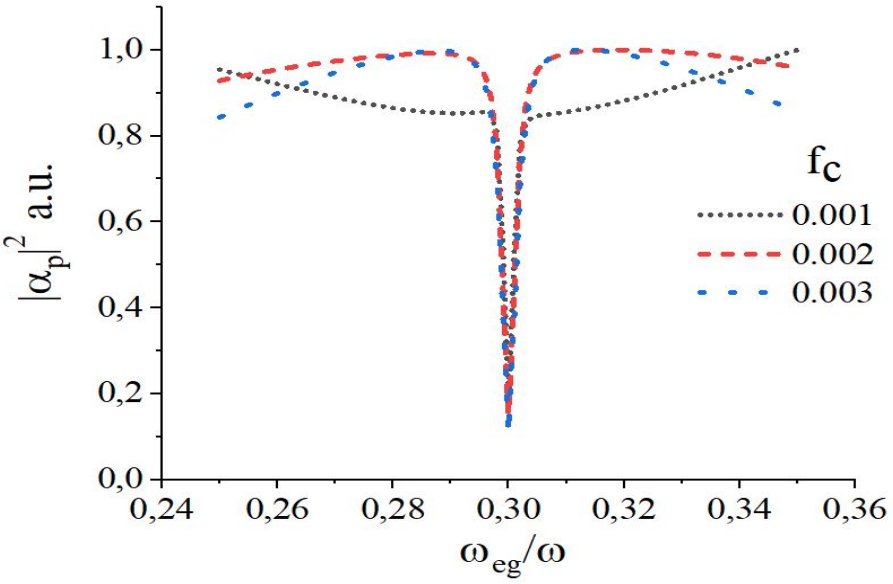

Figure 4.8: MNP plasmon intensity ($|\alpha_p|^2$) versus quantum emitter level-spacing ω_{eg} calculated for different values of the MNP-QE coupling strength f_c. We observe the suppression of the plasmon field at $\omega_{eg} = 0.3\omega$. Other parameters are $g = 0.01\omega$, $\gamma_p = 0.1\omega$, $\Omega_1 = \omega$, $\Omega_2 = 0.3\omega$, $\Omega_3 = 0.7\omega$, $\Omega_p = 0.3\omega$, $\gamma_1 = \gamma_2 = \gamma_3 = 5 \times 10^{-4}\ \omega$, $\gamma_{eg} = 10^{-5}\omega$, and $\chi_2 = 2 \times 10^{-9}\ \omega$.

In Fig. 4.8, we plot the MNP plasmon intensity ($|\alpha_p|^2$) versus level-spacing of the QE ω_{eg} for different f_c values. The plasmon intensity demonstrates a dip at ω_{eg}= 0.3ω.

When the Figs. 4.3 and 4.8 are compared, one can realize that a 300 times enhancement appears in the down-converted field $|\alpha_2|^2$, for $\omega_{eg} = 0.3\omega$, that is when the plasmon mode of the MNP is suppressed. Thus, it is natural to get suspicious if this 300 times enhancement occurs, actually, due to the suppression of the plasmon excitation around $\omega_{eg} = 0.3\omega$, i.e., when strong absorption of the MNP is turned off. We, such a suspicion in mind, checked our calculations several times. We inspected if we define the enhancement factor of $|\alpha_2|^2$, as a mistake, by comparing the two cases, i.e., when (i) MNP-QE dimer is present versus (ii) MNP is present alone. We confirmed that in our all results we compare the case (i) when MNP-QE dimer is present versus (ii) no particle is present (a bare crystal), i.e., the one in Eq. (4.19).

In Fig. 4.9 we change the parameters. After carrying out a neat inspection for the new parameters, we realize that, the maximum of the enhancement does not appear at $\omega_{eg} = 0.3\omega$,

but it appears at $\simeq 0.297\omega$. In Fig. 3.9(b), however, we observe that plasmon excitation is suppressed maximally still at $\omega_{eg} = 0.3\omega$. For other choices of the parameters f_c and g, one can see this discrimination more explicitly. That is, maximum $|\alpha_2|^2$ enhancement appears for an ω_{eg} which is apparently different than the $\omega_{eg} = 0.3\omega$ where plasmon absorption is suppressed.

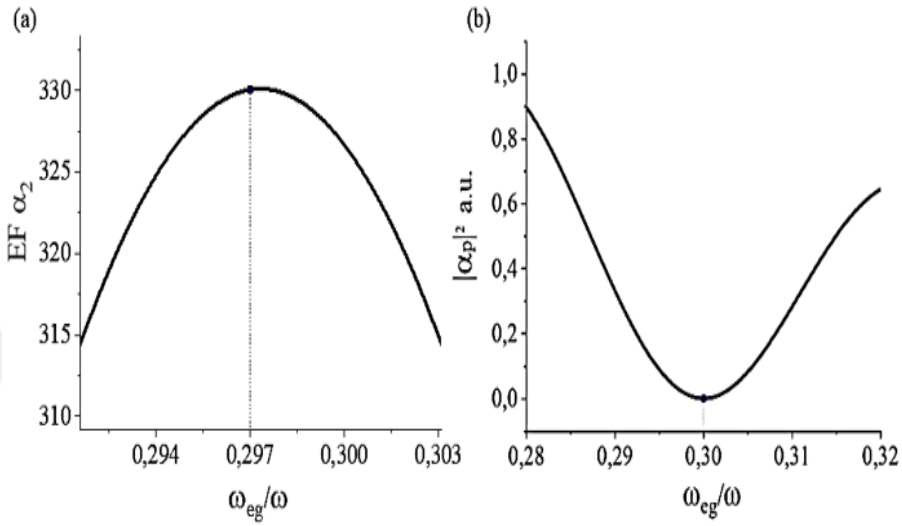

Figure 4.9: (a) Maximum enhancement factor is observed at $\omega_{eg} \simeq 0.297\omega$ for another choice of parameters. (b) Whereas, the maximum suppression of the MNP excitation is still at $\omega_{eg} = 0.3\omega$ for the new parameter set $\gamma_p = 0.01\ \omega$, $f_c = 0.03\omega$, $g = 0.1\omega$, $\Omega_1 = \omega$, $\Omega_2 = 0.3\omega$, $\Omega_3 = 0.7\omega$, $\Omega_p = 0.3\omega$, $\gamma_1 = \gamma_2 = \gamma_3 = 5 \times 10^{-4}\omega$, $\gamma_{eg} = 10^{-5}\omega$, and $\chi_2 = 2 \times 10^{-9}\omega$.

Actually, Ref. [89] too faces a similar situation, where second harmonic converting crystal embedded with MNP-QE dimers is studied. That is, maximum second harmonic generation (SHG) enhancement appears, again, near the converted frequency ($\omega_{eg} \simeq 2\omega$) where MNP excitation/absorption is suppressed. This led the authors of Ref. [89] a suspicion similar to the one here. In the study of nonlocalized response in Ref. [89], unlike the present study, authors managed to obtain a simple analytical form for the second harmonic field amplitude, which can explain such a behaviour. The path interference effects in an unlocalized nonlinear process, e.g. taking place in the body of a crystal, possess an *enriched* cancellation scheme [89] in the denominator. This is more sophisticated compared to the one where frequency conversion takes place at the hot spots [17]. Eq. 4.24 in the Appendix (Sec. 4.4), demonstrates that cancellations in the enriched denominator can take place when the QE

level-spacing is near the converted frequency, e.g., $\omega_{eg} \sim 2\ \omega$ in Ref. [89] or $\omega_{eg} \sim 0.3\omega$ here.

4.2.2 The idler intensity $|\alpha_3|^2$

The "*steady-state*" intensity of the other (idler) mode, α_3, gets almost unaffected from the enhancement of the α_2 mode. At first sight, this situation appears a bit counter-intuitive considering the argument (Arg.1) below. (Arg.1) Yes, the number conservation constraint, originating from the process $\hat{a}_3^\dagger \hat{a}_2^\dagger\ \hat{a}_1$, between the $|\alpha_2|^2$ and $|\alpha_3|^2$, is broken by the presence of the plasmonic (dimer) term in Eq. (4.11) and Eqs. (4.15-4.16). MNP-QE dimer couples only to the α_2 mode. In the frequency conversion process, however, the dimer can only absorb photons from the α_2 mode. Because the dimer is not pumped elsewhere. Thus, enhancement of $|\alpha_2|^2$ without altering the $|\alpha_3|^2$, at first may appear erratic? (Arg.2) Nevertheless, after noting that $|\alpha_{2,3}|^2$ are the "steady-state" values for the signal and idler, i.e., not the total number of generated photons, situation turns out to be reasonable [1].

While here we consider QEs for longer lifetime particles, coupled to the MNPs, they can also be replaced with metal nanostructures supporting long-life dark-modes. Actually, metal nanostructures, or even a single MNP structure, can support both bright and dark modes where the two modes interact with each other and result in Fano resonances [118, 23].

4.2.3 Retardation Effects

We note that the analytical model, we base our results on, does not take the retardation effects and increased density of modes into account. 3D FDTD solutions of Maxwell equations show that retardation effects do not destroy the appearance of Fano resonances when the nonlinearity takes place on (or close to) a nanoparticle [18, 89]. The case we study here, however, considers a nonlinearity conversion which takes place all over the nonlinear crystal,

[1] As an illuminating example: at linear Fano resonances the steady-state amplitude of the plasmon excitation is suppressed [64]. When the time evolution is considered, in contrary, Fano resonance creates much intense hot spots [26],[94]

i.e., not only on the hot spot. Thus, the retardation effects have to be revisited [2].

Actually, Ref. [89] managed to show that retardation effects do not wash out the path interference phenomenon. In Ref. [89], authors consider a setup, similar to the one in Fig. 4.1, but inspect the second harmonic generation process [3]. More explicitly, solutions of 3D nonlinear Maxwell equations show that an extra enhancement due to path interference multiplies the enhancement due to localization (of MNPs).

We also note that our basic model does not account the change (increase) in the density of modes appearing for a QE near MNP. Our aim in this chapter, already, is to study solely the path interference effects on the parametric down conversion process. In this thesis, we concentrate on the enhancement factors taking place due to the path interferences [3]. Our basic model cannot take into account the enhancements due to localization; thus, presents the ones due to path interference only.

4.3 Summary and Discussions

In this work, we study path interference effects in a nonlinear crystal generating down-converted signals. A long-life quantum emitter (QE), weakly interacting with the down-converted field alone, is made couple with the down-converted field over an MNP's hot spot. In other words, MNPs are utilized as interaction centers. Analytical results show that it is possible to strengthen the down-converted signal more than 2 orders of magnitude in a nonlinear crystal having an inherently weak output, when the parameters are chosen accordingly. We stress that this enhancement factor further multiplies the enhancement occurring due to the localization field (hot spot) enhancement.

The MNP-QE dimers are decorated on the surface of the nonlinear crystal. They couple to the down-converted field via evanescent waves (see Fig 4.1) where strong couplings are demonstrated to be achieved [119, 120, 121, 122]. This way, the level-spacing of the QEs

[2] Second harmonic process is encoded in many FDTD programs through the exact form of the nonlinear 3D Maxwell equations. The down-conversion process (neither, e.g., Raman conversion process), however, is not treated with exact solutions of nonlinear Maxwell equations, but their enhancement is predicted from the localization factors [8, 10, 9].

[3] 3D simulations in Ref. [89] shows that such effects are not washed out by retardation effects.

can be finely tuned via an applied voltage [53, 54, 123, 124, 125]. Fine tuning is crucial in Fano resonances. The presented interference scheme, controlling "unlocalized" nonlinear processes, necessitates much smaller coupling strengths compared to the one for local nonlinearities [17, 18].

In recent experiments [8, 10, 9] and the theoretical predictions [126, 127], the pumped cavity mode, Ω_1 mode, oscillating with $e^{-i\omega t}$, is coupled with the MNPs. Field localization effect of MNP is utilized [8, 10, 9]. In the present study, in difference, the MNPs couple with the down-converted signal $\omega_2 = 0.3\omega$. The present work can neither treat the enhancement due to localization. Because it does not conduct a simulation of 3D Maxwell equations. The localization effect is referred only as strong light-MNP and MNP-QE couplings.

Retardation effects, in the studied system, can be more demolishing compared to the ones for a localized nonlinear conversion process. Yet, a very recently [89] study demonstrates that retardation effects do not wash out the path interference phenomenon, in a second harmonic converting crystal (see also Appendix). Our work presents the first demonstration of the path interference effect in a spontaneous down-converting nonlinear crystal.

While the actual aim of this work is to see the path interference effects, i.e., disassociating the effects of the localization, we can propose the following schemes for achieving much stronger spontaneous down conversion enhancements. Using a metal nanostructure, supporting two plasmon modes resonant to $\omega_1 = \omega$ and $\omega_2 = 0.3\omega$, could enhance the down conversion process (i) by localizing both fields and (ii) by controlling the enhancement via path interference the QE (ω_{eg}) creates around the lower-energy plasmon mode[4], near $\omega_2 = 0.3\omega$. Still, the path interference enhancement multiplies the localization enhancement.

The interference scheme, we study here, presents several advantages compared to the ones utilizing merely the local field enhancement effect. (i) The signal intensity can be enhanced 2 orders without enhancing the fundamental field. This enables further enhancements for devices already operating near the break down temperatures. (ii) The scheme can be used together with the local field enhancement schemes. (iii) One can enhance merely the signal intensity without increasing the idler frequency. (iv) The scheme can also be used for sup-

[4]This is a double-resonance scheme [94]. A triple resonance scheme can be further considered for much stronger enhancement.

pressing the nonlinearities. (v) Above all, the tunability of the QEs' level-spacing enables turning ON and OFF of the enhancement and suppression via an applied voltage for further applications.

While Fano resonances provide a narrowband enhancement, suppression and control mechanism; FRs enable this operation with small QE level-spacing tunings. Thus, gaining control over these phenomena or even developing an understanding on them have crucial importance in the development of new quantum technologies.

4.4 Appendix

Ref. [89], studies the control (in particular enhancement) of second harmonic process in a nonlinear cavity, via MNP-QE dimers, both analytically and by exact solution of 3D Maxwell equations. In that upconverting system, authors are able to obtain a simple expression for the SH field amplitude, say β_2, in terms of the first harmonic amplitude

$$\tilde{\beta}_2 = \frac{-i\chi_2}{[i(\Omega_2 - 2\omega) + \gamma_2] + \frac{|g|^2}{[i(\Omega_p - 2\omega) + \gamma_p] - \frac{|f_p|^2 y}{[i(\omega_{eg} - 2\omega) + \gamma_{eg}]}}} \tilde{\beta}_1^2. \tag{4.24}$$

Eq. (4.24) reveals , in Ref. [89], how upconversion enhancement or suppression take place. Simply, (i) cancellations in the denominator (call as path interference) reduce the denominator resulting an enhanced SHG. In contrary, (ii) cancellations can also enlarge denominator at certain parameters where a suppression in the SHG is obtained.

In Ref. [89], Eq. (4.24) can envisage the exact solution of 3D Maxwell equations (FEM simulations) perfectly. Thus, one can also clearly witness that the predicted resonances are not washed out by retardation effects in the path interference control of an unlocalized process.

FEM simulations [89] also clearly demonstrates that SHG enhancement can take place without any local field enhancement.

Enhancement near $\omega_{eg} \simeq \omega_{\rm NL} = 2\omega$.— In Eq. (4.24), one can see that $|f_p|^2 y/[\ldots]$ term becomes sufficiently large near $\omega_{eg} \simeq \omega_{\rm NL} = 2\omega$. Hence, in this regime it can create a cancellation with the $[i(\Omega_p - 2\omega) + \gamma_p]$ term, making $|g|^2/(\ldots)$ term sufficiently large for performing cancellation in the $[i(\Omega_2 - 2\omega) + \gamma_2]$ term. Consequently, the denominator of β_2 can become smaller.

This argument explains why authors obtain SHG enhancement near $\omega_{eg} \simeq \omega_{\rm NL} = 2\omega$ in Ref. [89], a phenomenon also appearing in this work. In the presented work, however, we cannot manage to obtain such an analytical expression.

5 CONCLUSIONS

In this thesis, Fano-control of the steady-state nonlinear processes was studied. In the first part, we worked on a local nonlinear (second harmonic generation, SHG) process taking place at a hot spot [31]. Then, we studied the control of unlocalized spontaneous down conversion processes taking place in the body of a frequency converting crystal via utilizing MNPs as interaction centers [**?**].

A control mechanism for both enhancement and suppression of the SHG response is beneficial. The SHG signal can be adjusted both controlling the linear and nonlinear response. We demonstrate that one can gain control over the steady-state second harmonic signal from a plasmonic nano-material via two kinds of FRs. Fano resonances utilized to control (a) the linear and (b) the nonlinear responses. We showed that steady-state SHG, taking place at a hot spot, can control (in particular enhance) the linear signal. In method (b), Fano resonance in the nonlinear response, we showed that to how to control (enhance and suppress) the SHG without modifiying the linear response, i.e., the hot spot field. The exact solution of Maxwell equations obtained by FDTD simulations matched with our analytical model. We demonstrated that the SHG suppression, predicted by the analytical model, is observable in FDTD simulations.

We study the nonlinear response of a down-converting crystal which MNP-QE dimers placed on its surface. The MNPs on the crystal surface make the unlocalized down-converted field concentrate into the hot spots where a stronger interaction with a quantum emitter takes place. We showed that our setup could enhance the down-converted field 2 orders of magnitude with quite weak interaction strengths. This enhancement comes as a further multiplication factor on top of the enhancement originates from the MNP hot spot enhancement.

References

[1] Robert W. Boyd. *Nonlinear Optics*. Elsevier, **2003**.

[2] Mark I. Stockman. Nanoplasmonics: past, present, and glimpse into future. *Optics Express*, 19(22):22029–22106, **2011**.

[3] Xiaohua Wu, Stephen K Gray, and Matthew Pelton. Quantum-dot-induced transparency in a nanoscale plasmonic resonator. *Optics Express*, 18(23):23633–23645.

[4] Christiane Höppener, Zachary J Lapin, Palash Bharadwaj, and Lukas Novotny. Self-similar gold-nanoparticle antennas for a cascaded enhancement of the optical field. *Physical Review Letters*, 109(1):017402, **2012**.

[5] Eric Le Ru and Pablo Etchegoin. *Principles of Surface-Enhanced Raman Spectroscopy: and related plasmonic effects*. Elsevier, **2008**.

[6] Ming-Liang Ren, Si-Yun Liu, Ben-Li Wang, Bao-Qin Chen, Jiafang Li, and Zhi-Yuan Li. Giant enhancement of second harmonic generation by engineering double plasmonic resonances at nanoscale. *Optics Express*, 22(23):28653–28661, **2014**.

[7] Ekaterina Poutrina, Cristian Ciracì, Daniel J Gauthier, and David R Smith. Enhancing four-wave-mixing processes by nanowire arrays coupled to a gold film. *Optics Express*, 20(10):11005–11013, **2012**.

[8] WJ Nie, YX Zhang, HH Yu, Rang Li, RY He, NN Dong, Roman Wang, Jun, SQ Zhou, et al. Plasmonic nanoparticles embedded in single crystals synthesized by gold ion implantation for enhanced optical nonlinearity and efficient q-switched lasing. *Nanoscale*, 10(9):4228–4236, **2018**.

[9] Rang Li, Ningning Dong, Chen Cheng, Feng Ren, René Hübner, Jun Wang, Shengqiang Zhou, and Feng Chen. Giant enhancement of nonlinear optical response in nd: Yag single crystals by embedded silver nanoparticles. *ACS Omega*, 2(4):1279–1286, **2017**.

[10] Yingying Wang, Yixiao Niu, Gang Wang, Yongjie Sun, and Changlong Liu. Enhanced nonlinear optical properties of LiNbO3 crystal embedded with cuzn alloy nanoparticles by ion implantation. *Journal of Alloys and Compounds*, 778:691–698, **2019**.

[11] Eugene Kamenetskii, Almas Sadreev, and Andrey Miroshnichenko. *Fano Resonances in Optics and Microwaves*. Springer, **2018**.

[12] Marlan O. Scully and M. Suhail Zubairy. *Quantum Optics*. American Association of Physics Teachers, **1999**.

[13] Ali Panahpour, Abolfazl Mahmoodpoor, and Andrei V Lavrinenko. Refraction enhancement in plasmonics by coherent control of plasmon resonances. *Physical Review B*, 100(7):075427, **2019**.

[14] Mehmet Günay, You-Lin Chuang, and Mehmet Emre Tasgin. Continuously-tunable cherenkov-radiation-based detectors via plasmon index control. *Nanophotonics*, 9(6):1479–1489, **2020**.

[15] Emre Yuce, Zafer Artvin, Ramazan Sahin, Alpan Bek, and Mehmet Emre Tasgin. Ultra-large actively tunable photonic band gaps via plasmon-analog of index enhancement. *arXiv preprint arXiv:2006.07132*, **2020**.

[16] Jérémy Butet and Olivier JF Martin. Fano resonances in the nonlinear optical response of coupled plasmonic nanostructures. *Optics Express*, 22(24):29693–29707, **2014**.

[17] Deniz Turkpence, Gursoy B Akguc, Alpan Bek, and Mehmet Emre Tasgin. Engineering nonlinear response of nanomaterials using fano resonances. *Journal of Optics*, 16(10):105009, **2014**.

[18] Mehmet Emre Taşgın, Alpan Bek, and Selen Postacı. Fano resonances in the linear and nonlinear plasmonic response. In *Fano Resonances in Optics and Microwaves*, pages 1–31. Springer, **2018**.

[19] Mehmet Emre Tasgin, Alpan Bek, and Selen Postaci. Fano resonances in optics and microwaves: Physics and application. *Springer Series in Optical Sciences*, **2018**.

[20] Shailendra K Singh, M Kurtulus Abak, and Mehmet Emre Tasgin. Enhancement of four-wave mixing via interference of multiple plasmonic conversion paths. *Physical Review B*, 93(3):035410, **2016**.

[21] SM. Sadeghi, WJ. Wing, and RR. Gutha. Undamped ultrafast pulsation of plasmonic fields via coherent exciton-plasmon coupling. *Nanotechnology*, 26(8):085202, **2015**.

[22] Mohamed ElKabbash, Alireza R Rashed, Betul Kucukoz, Quang Nguyen, Ahmet Karatay, Gul Yaglioglu, Ekmel Ozbay, Humeyra Caglayan, and Giuseppe Strangi. Ultrafast transient optical loss dynamics in exciton–plasmon nanoassemblies. *Nanoscale*, 9(19):6558–6566, **2017**.

[23] Bilge Can Yildiz, Alpan Bek, and Mehmet Emre Tasgin. Plasmon lifetime enhancement in a bright-dark mode coupled system. *Physical Review B*, 101(3):035416, **2020**.

[24] Rasim Volga Ovali, Ramazan Sahin, Alpan Bek, and Mehmet Emre Tasgin. Single-molecule-resolution ultrafast near-field optical microscopy via plasmon lifetime extension. *arXiv preprint arXiv:2007.01131*, **2020**.

[25] Mehmet Emre Taşgın. Metal nanoparticle plasmons operating within a quantum lifetime. *Nanoscale*, 5(18):8616–8624, **2013**.

[26] Mark I. Stockman. Nanoscience: Dark-hot resonances. *Nature*, 467(7315):541, **2010**.

[27] Yu Zhang, Fangfang Wen, Yu-Rong Zhen, Peter Nordlander, and Naomi J. Halas. Coherent Fano resonances in a plasmonic nanocluster enhance optical four-wave mixing. *Proceedings of the National Academy of Sciences*, 110(23):9215–9219, **2013**.

[28] Yu Zhang, Yu-Rong Zhen, Oara Neumann, Jared K Day, Peter Nordlander, and Naomi J Halas. Coherent anti-Stokes Raman scattering with single-molecule sensitivity using a plasmonic Fano resonance. *Nature Communications*, 5(1):1–7, **2014**.

[29] Mark I. Stockman. The spaser as a nanoscale quantum generator and ultrafast amplifier. *Journal of Optics*, 12(2):024004, **2010**.

[30] MA Noginov, G Zhu, AM Belgrave, Reuben Bakker, VM Shalaev, EE Narimanov, S Stout, E Herz, T Suteewong, and U Wiesner. Demonstration of a spaser-based nanolaser. *Nature*, 460(7259):1110–1112, **2009**.

[31] Mehmet Günay, Zafer Artvin, Alpan Bek, and Mehmet Emre Tasgin. Controlling steady-state second harmonic signal via linear and nonlinear fano resonances. *Journal of Modern Optics*, 67(1):26–34, **2020**.

[32] H. Ishizuki, T. Suhara, M. Fujimura, and H. Nishihara. Wavelength-conversion type picosecond optical switching using a waveguide qpm-shg/dfg device. *Optical and Quantum Electronics*, 33(7-10):953–961, **2001**.

[33] RJ Horowicz. Quantum correlation between fundamental and second harmonic in shg. *EPL (Europhysics Letters)*, 10(6):537, **1989**.

[34] Auro M. Perego, Sergei K. Turitsyn, and Kestutis Staliunas. Gain through losses in nonlinear optics. *Light: Science & Applications*, 7(1):1–11, **2018**.

[35] Yu-hua Wang, Xiang-xiang Yu, Fei Liu, and Yu-mei Wang. Nonlinear refraction of lithium niobate crystal doped with different metal nanoparticles. *Materials Letters*, 123:35–37, **2014**.

[36] David N Nikogosyan. *Nonlinear optical crystals: a complete survey*. Springer Science & Business Media, **2006**.

[37] Paul G. Kwiat, Klaus Mattle, Harald Weinfurter, Anton Zeilinger, Alexander V. Sergienko, and Yanhua Shih. New high-intensity source of polarization-entangled photon pairs. *Physical Review Letters*, 75(24):4337, **1995**.

[38] Artur K. Ekert. Quantum cryptography based on Bell's theorem. *Physical Review Letters*, 67(6):661, **1991**.

[39] Adriano Barenco, David Deutsch, Artur Ekert, and Richard Jozsa. Conditional quantum dynamics and logic gates. *Physical Review Letters*, 74(20):4083, **1995**.

[40] S. Euler, M. Beier, M. Sinther, and Th. Walther. Spontaneous parametric down-conversion in waveguide chips for quantum information. In *AIP Conference Proceedings*, volume 1363, pages 323–326. American Institute of Physics, 2011.

[41] T. Trupke, M.A. Green, and P. Würfel. Improving solar cell efficiencies by down-conversion of high-energy photons. *Journal of Applied Physics*, 92(3):1668–1674, **2002**.

[42] Ze'ev R. Abrams, Avi Niv, and Xiang Zhang. Solar energy enhancement using down-converting particles: A rigorous approach. *Journal of Applied Physics*, 109(11):114905, **2011**.

[43] Jianwei Wang, Fabio Sciarrino, Anthony Laing, and Mark G Thompson. Integrated photonic quantum technologies. *Nature Photonics*, pages 1–12, **2019**.

[44] Jeremy L. O'brien, Akira Furusawa, and Jelena Vučković. Photonic quantum technologies. *Nature Photonics*, 3(12):687, **2009**.

[45] Sergey I. Bozhevolnyi and N. Asger Mortensen. Plasmonics for emerging quantum technologies. *Nanophotonics*, 6(5):1185–1188, **2017**.

[46] James Schneeloch and John C Howell. Introduction to the transverse spatial correlations in spontaneous parametric down-conversion through the biphoton birth zone. *Journal of Optics*, 18(5):053501, **2016**.

[47] MV Jabir and GK Samanta. Robust, high brightness, degenerate entangled photon source at room temperature. *Scientific reports*, 7(1):12613, **2017**.

[48] Aitor Villar, Alexander Lohrmann, and Alexander Ling. Experimental entangled photon pair generation using crystals with parallel optical axes. *Optics Express*, 26(10):12396–12402, **2018**.

[49] Zafer Artvin, Mehmet Gunay, Alpan Bek, and Mehmet Emre Tasgin. Fano-control of down-conversion in a nonlinear crystal via plasmonic–quantum emitter hybrid structures. *JOSA B*, 37(12):3769–3776, **2020**.

[50] Lukas Novotny and Bert Hecht. *Principles of nano-optics*. Cambridge university press, **2012**.

[51] Artur Zrenner, E Beham, S Stufler, F Findeis, M Bichler, and Gerhard Abstreiter. Coherent properties of a two-level system based on a quantum-dot photodiode. *Nature*, 418(6898):612–614, **2002**.

[52] Tomas Edvinsson. Optical quantum confinement and photocatalytic properties in two-, one-and zero-dimensional nanostructures. *Royal Society Open Science*, 5(9):180387, **2018**.

[53] MJ Conterio, N Sköld, DJP Ellis, I Farrer, DA Ritchie, and AJ Shields. A quantum dot single photon source driven by resonant electrical injection. *Applied Physics Letters*, 103(16):162108, **2013**.

[54] Saniya Deshpande, Junseok Heo, Ayan Das, and Pallab Bhattacharya. Electrically driven polarized single-photon emission from an ingan quantum dot in a gan nanowire. *Nature Communications*, 4(1):1–8, **2013**.

[55] Florent Simon, Simon Clevers, Valerie Dupray, and Gerard Coquerel. Relevance of the second harmonic generation to characterize crystalline samples. *Chemical Engineering & Technology*, 38(6):971–983, **2015**.

[56] PA Franken, Alan E Hill, CW el Peters, and G Weinreich. Generation of optical harmonics. *Physical Review Letters*, 7(4):118, **1961**.

[57] Theodore H Maiman. Stimulated optical radiation in ruby. *nature*, 187(4736):493–494, **1960**.

[58] Thomas Brabec and Ferenc Krausz. Intense few-cycle laser fields: Frontiers of nonlinear optics. *Reviews of Modern Physics*, 72(2):545, **2000**.

[59] G Kh Kitaeva and Aleksandr Nikolaevich Penin. Spontaneous parametric down-conversion. *Journal of Experimental and Theoretical Physics Letters*, 82(6):350–355, **2005**.

[60] Yuan Li, Fei Ding, and Oliver G Schmidt. Entangled-photons generation with quantum dots. *Chinese Physics B*, 27(2):020307, **2018**.

[61] Koenraad MR Audenaert, John Calsamiglia, Ramón Munoz-Tapia, Emilio Bagan, Ll Masanes, Antonio Acin, and Frank Verstraete. Discriminating states: The quantum chernoff bound. *Physical Review Letters*, 98(16):160501, **2007**.

[62] L Caspani, C. Xiong, BJ Eggleton, D. Bajoni, M. Liscidini, M. Galli, R. Morandotti, and DJ. Moss. Integrated sources of photon quantum states based on nonlinear optics. In *Appl*, volume 6, page e17100, **2017**.

[63] Ugo Fano. Effects of configuration interaction on intensities and phase shifts. *Physical Review*, 124(6):1866, **1961**.

[64] Mikhail F. Limonov, Mikhail V. Rybin, Alexander N Poddubny, and Yuri S Kivshar. Fano resonances in photonics. *Nature Photonics*, 11(9):543–554, **2017**.

[65] Boris Luk'yanchuk, Nikolay I Zheludev, Stefan A Maier, Naomi J Halas, Peter Nordlander, Harald Giessen, and Chong Tow Chong. The fano resonance in plasmonic nanostructures and metamaterials. *Nature Materials*, 9(9):707–715, **2010**.

[66] King Yan Fong, Linran Fan, Liang Jiang, Xu Han, and Hong X Tang. Microwave-assisted coherent and nonlinear control in cavity piezo-optomechanical systems. *Physical Review A*, 90(5):051801, **2014**.

[67] Pengyu Fan, Zongfu Yu, Shanhui Fan, and Mark L. Brongersma. Optical fano resonance of an individual semiconductor nanostructure. *Nature materials*, 13(5):471–475, **2014**.

[68] Andrey E Miroshnichenko, Sergej Flach, and Yuri S Kivshar. Fano resonances in nanoscale structures. *Reviews of Modern Physics*, 82(3):2257, **2010**.

[69] Xueqin Huang, Yun Lai, Zhi Hong Hang, Huihuo Zheng, and CT Chan. Dirac cones induced by accidental degeneracy in photonic crystals and zero-refractive-index materials. *Nature Materials*, 10(8):582–586, **2011**.

[70] Parikshit Moitra, Yuanmu Yang, Zachary Anderson, Ivan I. Kravchenko, Dayrl P. Briggs, and Jason Valentine. Realization of an all-dielectric zero-index optical metamaterial. *Nature Photonics*, 7(10):791–795, **2013**.

[71] Petru Ghenuche, Grégory Vincent, Marine Laroche, Nathalie Bardou, Riad Haïdar, Jean-Luc Pelouard, and Stéphane Collin. Optical extinction in a single layer of nanorods. *Physical Review Letters*, 109(14):143903, **2012**.

[72] Nanfang Yu and Federico Capasso. Flat optics with designer metasurfaces. *Nature Materials*, 13(2):139–150, **2014**.

[73] CL Garrido Alzar, MAG Martinez, and P Nussenzveig. Classical analog of electromagnetically induced transparency. *American Journal of Physics*, 70(1):37–41, **2002**.

[74] Philippe Tassin, Lei Zhang, Th Koschny, EN Economou, and Costas M Soukoulis. Low-loss metamaterials based on classical electromagnetically induced transparency. *Physical Review Letters*, 102(5):053901, **2009**.

[75] Na Liu, Lutz Langguth, Thomas Weiss, Jürgen Kästel, Michael Fleischhauer, Tilman Pfau, and Harald Giessen. Plasmonic analogue of electromagnetically induced transparency at the drude damping limit. *Nature Materials*, 8(9):758–762, **2009**.

[76] SM. Sadeghi, WJ Wing, and RR. Gutha. Undamped ultrafast pulsation of plasmonic fields via coherent exciton-plasmon coupling. *Nanotechnology*, 26(8):085202, **2015**.

[77] Mohamed ElKabbash, Alireza R Rashed, Betul Kucukoz, Quang Nguyen, Ahmet Karatay, Gul Yaglioglu, Ekmel Ozbay, Humeyra Caglayan, and Giuseppe Strangi. Ultrafast transient optical loss dynamics in exciton–plasmon nanoassemblies. *Nanoscale*, 9(19):6558–6566, **2017**.

[78] Jinna He, Chunzhen Fan, Pei Ding, Shuangmei Zhu, and Erjun Liang. Near-field engineering of fano resonances in a plasmonic assembly for maximizing cars enhancements. *Scientific Reports*, 6:20777, **2016**.

[79] Jian Ye, Fangfang Wen, Heidar Sobhani, J Britt Lassiter, Pol Van Dorpe, Peter Nordlander, and Naomi J Halas. Plasmonic nanoclusters: near field properties of the fano resonance interrogated with sers. *Nano letters*, 12(3):1660–1667, **2012**.

[80] Selen Postaci, Bilge Can Yildiz, Alpan Bek, and Mehmet Emre Tasgin. Silent enhancement of sers signal without increasing hot spot intensities. *Nanophotonics*, 7(10):1687–1695, **2018**.

[81] Dana E Westmoreland, Kevin P McClelland, Kaitlyn A Perez, James C Schwabacher, Zhengyi Zhang, and Emily A Weiss. Properties of quantum dots coupled to plasmons and optical cavities. *The Journal of Chemical Physics*, 151(21):210901, **2019**.

[82] James T. Hugall, Anshuman Singh, and Niek F. van Hulst. Plasmonic cavity coupling. *ACS Photonics*, 5(1):43–53, **2018**.

[83] Kotni Santhosh, Ora Bitton, Lev Chuntonov, and Gilad Haran. Vacuum rabi splitting in a plasmonic cavity at the single quantum emitter limit. *Nature Communications*, 7(1):1–5, **2016**.

[84] Haixu Leng, Brian Szychowski, Marie-Christine Daniel, and Matthew Pelton. Strong coupling and induced transparency at room temperature with single quantum dots and gap plasmons. *Nature Communications*, 9(1):1–7, **2018**.

[85] Salvatore Savasta, Rosalba Saija, Alessandro Ridolfo, Omar Di Stefano, Paolo Denti, and Ferdinando Borghese. Nanopolaritons: vacuum rabi splitting with a single quantum dot in the center of a dimer nanoantenna. *ACS Nano*, 4(11):6369–6376, **2010**.

[86] Haifeng Yuan, Saumyakanti Khatua, Peter Zijlstra, Mustafa Yorulmaz, and Michel Orrit. Thousand-fold enhancement of single-molecule fluorescence near a single gold nanorod. *Angewandte Chemie*, 125(4):1255–1259, **2013**.

[87] Pascal Anger, Palash Bharadwaj, and Lukas Novotny. Enhancement and quenching of single-molecule fluorescence. *Physical Review Letters*, 96(11):113002, **2006**.

[88] Song-Yuan Ding, Jun Yi, Jian-Feng Li, Bin Ren, De-Yin Wu, Rajapandiyan Panneerselvam, and Zhong-Qun Tian. Nanostructure-based plasmon-enhanced raman spectroscopy for surface analysis of materials. *Nature Reviews Materials*, 1(6):1–16, **2016**.

[89] Mehmet Günay, Ahmet Cicek, Nurettin Korozlu, Alpan Bek, and Mehmet Emre Taşgın. Fano control of unlocalized nonlinear processes. *arXiv preprint arXiv:1905.01129*, **2019**.

[90] Niels Verellen, Yannick Sonnefraud, Heidar Sobhani, Feng Hao, Victor V Moshchalkov, Pol Van Dorpe, Peter Nordlander, and Stefan A Maier. Fano resonances in individual coherent plasmonic nanocavities. *Nano Letters*, 9(4):1663–1667, **2009**.

[91] J Butet, G Bachelier, I. Russier-Antoine, F Bertorelle, A Mosset, N Lascoux, C Jonin, E Benichou, and P-F Brevet. Nonlinear fano profiles in the optical second-harmonic generation from silver nanoparticles. *Physical Review B*, 86(7):075430, **2012**.

[92] Krishnan Thyagarajan, Jérémy Butet, and Olivier JF Martin. Augmenting second harmonic generation using fano resonances in plasmonic systems. *Nano Letters*, 13(4):1847–1851, **2013**.

[93] Johann Berthelot, Guillaume Bachelier, Mingxia Song, Padmnabh Rai, Gérard Colas Des Francs, Alain Dereux, and Alexandre Bouhelier. Silencing and enhancement of second-harmonic generation in optical gap antennas. *Optics Express*, 20(10):10498–10508, **2012**.

[94] Yizhuo Chu, Mohamad G Banaee, and Kenneth B Crozier. Double-resonance plasmon substrates for surface-enhanced Raman scattering with enhancement at excitation and Stokes frequencies. *ACS nano*, 4(5):2804–2810, **2010**.

[95] Bilge Can Yildiz, Mehmet Emre Tasgin, Musa Kurtulus Abak, Sahin Coskun, Husnu Emrah Unalan, and Alpan Bek. Enhanced second harmonic generation from coupled asymmetric plasmonic metal nanostructures. *Journal of Optics*, 17(12):125005, **2015**.

[96] Mehmet Emre Tasgin, Ildar Salakhutdinov, Dania Kendziora, Musa Kurtulus Abak, Deniz Turkpence, Luca Piantanida, Ljiljana Fruk, Marco Lazzarino, and Alpan Bek. Fluorescence excitation by enhanced plasmon upconversion under continuous wave illumination. *Photonics and Nanostructures-Fundamentals and Applications*, 21:32–43, **2016**.

[97] Kane Yee. Numerical solution of initial boundary value problems involving maxwell's equations in isotropic media. *IEEE Transactions on Antennas and Propagation*, 14(3):302–307, **1966**.

[98] Dennis M Sullivan. *Electromagnetic simulation using the FDTD method*. John Wiley & Sons, **2013**.

[99] Marco Finazzi and Franco Ciccacci. Plasmon-photon interaction in metal nanoparticles: second-quantization perturbative approach. *Physical Review B*, 86(3):035428, **2012**.

[100] Nicolai B Grosse, Jan Heckmann, and Ulrike Woggon. Nonlinear plasmon-photon interaction resolved by k-space spectroscopy. *Physical Review Letters*, 108(13):136802, **2012**.

[101] Sarina Wunderlich and Ulf Peschel. Plasmonic enhancement of second harmonic generation on metal coated nanoparticles. *Optics Express*, 21(16):18611–18623, **2013**.

[102] Malin Premaratne and Mark I. Stockman. Theory and technology of spasers. *Advances in Optics and Photonics*, 9(1):79–128, **2017**.

[103] Bumki Min, Eric Ostby, Volker Sorger, Erick Ulin-Avila, Lan Yang, Xiang Zhang, and Kerry Vahala. High-q surface-plasmon-polariton whispering-gallery microcavity. *Nature*, 457(7228):455–458, **2009**.

[104] Spyridon G Kosionis, Andreas F Terzis, Seyed M Sadeghi, and Emmanuel Paspalakis. Optical response of a quantum dot–metal nanoparticle hybrid interacting with a weak probe field. *Journal of Physics: Condensed Matter*, 25(4):045304, **2012**.

[105] FDTD Lumerical. Solutions, inc, **2018**.

[106] Peter B Johnson and R-WJPrB Christy. Optical constants of the noble metals. *Physical Review B*, 6(12):4370, **1972**.

[107] Jean-Pierre Berenger et al. A perfectly matched layer for the absorption of electromagnetic waves. *Journal of computational physics*, 114(2):185–200, **1994**.

[108] Umran S Inan and Robert A Marshall. *Numerical electromagnetics: the FDTD method*. Cambridge University Press, **2011**.

[109] Fuchyi Yang and Brian T. Cunningham. Enhanced quantum dot optical down-conversion using asymmetric 2d photonic crystals. *Optics Express*, 19(5):3908–3918, **2011**.

[110] Uttam Paudel, Jia Jun Wong, Michael Goggin, Paul G. Kwiat, Allan S. Bracker, Michael Yakes, Daniel Gammon, and Duncan G Steel. Direct excitation of a single quantum dot with cavity-spdc photons. *Optics Express*, 27(11):16308–16319, **2019**.

[111] Luciana RP Kassab, Cid B de Araújo, Renata A Kobayashi, Ricardo de Almeida Pinto, and Davinson M da Silva. Influence of silver nanoparticles in the luminescence efficiency of pr 3+-doped tellurite glasses. *Journal of Applied Physics*, 102(10):103515, **2007**.

[112] Ishita Mukherjee, Ghazal Hajisalem, and Reuven Gordon. One-step integration of metal nanoparticle in photonic crystal nanobeam cavity. *Optics Express*, 19(23):22462–22469, **2011**.

[113] Laurent Bigot, Hicham El Hamzaoui, Antoine Le Rouge, Géraud Bouwmans, Fernand Chassagneux, Bruno Capoen, and Mohamed Bouazaoui. Linear and nonlinear optical properties of gold nanoparticle-doped photonic crystal fiber. *Optics Express*, 19(20):19061–19066, **2011**.

[114] WJ Nie, YX Zhang, HH Yu, Rang Li, RY He, NN Dong, Jun Wang, René Hübner, Roman Böttger, SQ Zhou, et al. Plasmonic nanoparticles embedded in single crystals synthesized by gold ion implantation for enhanced optical nonlinearity and efficient q-switched lasing. *Nanoscale*, 10(9):4228–4236, **2018**.

[115] Rang Li, Ningning Dong, Chen Cheng, Feng Ren, René Hübner, Jun Wang, Shengqiang Zhou, and Feng Chen. Giant enhancement of nonlinear optical response in nd: Yag single crystals by embedded silver nanoparticles. *ACS Omega*, 2(4):1279–1286, **2017**.

[116] Ishita Mukherjee, Ghazal Hajisalem, and Reuven Gordon. One-step integration of metal nanoparticle in photonic crystal nanobeam cavity. *Optics Express*, 19(23):22462–22469, **2011**.

[117] Laurent Bigot, Hicham El Hamzaoui, Antoine Le Rouge, Géraud Bouwmans, Fernand Chassagneux, Bruno Capoen, and Mohamed Bouazaoui. Linear and nonlinear optical properties of gold nanoparticle-doped photonic crystal fiber. *Optics Express*, 19(20):19061–19066, **2011**.

[118] Simone Panaro, Adnan Nazir, Carlo Liberale, Gobind Das, Hai Wang, Francesco De Angelis, Remo Proietti Zaccaria, Enzo Di Fabrizio, and Andrea Toma. Dark to bright mode conversion on dipolar nanoantennas: a symmetry-breaking approach. *ACS Photonics*, 1(4):310–314, **2014**.

[119] Mickaël Février, Philippe Gogol, Abdelhanin Aassime, Robert Mégy, Cécile Delacour, Alexei Chelnokov, Aniello Apuzzo, Sylvain Blaize, Jean-Michel Lourtioz, and Béatrice Dagens. Giant coupling effect between metal nanoparticle chain and optical waveguide. *Nano letters*, 12(2):1032–1037, **2012**.

[120] Giovanni Magno, Mickael Fevrier, Philippe Gogol, Abdelhanin Aassime, Alexandre Bondi, Robert Mégy, and Béatrice Dagens. Strong coupling and vortexes assisted slow light in plasmonic chain-soi waveguide systems. *Scientific Reports*, 7(1):1–11, **2017**.

[121] Ibrahim Abdulhalim. Coupling configurations between extended surface electromagnetic waves and localized surface plasmons for ultrahigh field enhancement. *Nanophotonics*, 7(12):1891–1916, **2018**.

[122] F Hao and P Nordlander. Plasmonic coupling between a metallic nanosphere and a thin metallic wire. *Applied physics letters*, 89(10):103101, **2006**.

[123] S Schwarz, A Kozikov, F Withers, JK Maguire, AP Foster, S Dufferwiel, L Hague, MN Makhonin, LR Wilson, AK Geim, et al. Electrically pumped single-defect light emitters in wse2. *2D Materials*, 3(2):025038, **2016**.

[124] Alexander Högele, Stefan Seidl, Martin Kroner, Khaled Karrai, Richard J Warburton, Brian D Gerardot, and Pierre M Petroff. Voltage-controlled optics of a quantum dot. *Physical review letters*, 93(21):217401, **2004**.

[125] Jonas Fransson, M-G Kang, Y Yoon, S Xiao, Y Ochiai, JL Reno, N Aoki, and JP Bird. Tuning the fano resonance with an intruder continuum. *Nano Letters*, 14(2):788–793, **2014**.

[126] A. Loot, I. Sildos, and V. Hizhnyakov. Enhanced spontaneous parametric down-conversion in a metal-dielectric interface. In *2015 9th International Congress on Advanced Electromagnetic Materials in Microwaves and Optics (Metamaterials)*, pages 451–453. IEEE, **2015**.

[127] A. Loot and V. Hizhnyakov. Modeling of enhanced spontaneous parametric down-conversion in plasmonic and dielectric structures with realistic waves. *Journal of Optics*, 20(5):055502, 2018.

ATTACHMENTS

PUBLICATIONS

1. Zafer Artvin, Mehmet Gunay, Alpan Bek, and Mehmet Emre Tasgin, ”Fano-control of down-conversion in a nonlinear crystal via plasmonic–quantum emitter hybrid structures,” J. Opt. Soc. Am. B 37, 3769-3776 (2020) (2020) [49].

2. Mehmet Günay, Zafer Artvin, Alpan Bek and Mehmet Emre Tasgin (2020) Controlling steady-state second harmonic signal via linear and nonlinear Fano resonances, Journal of Modern Optics, 67:1, 26-34,

HACETTEPE UNIVERSITY
GRADUATE SCHOOL OF SCIENCE AND ENGINEERING
THESIS/DISSERTATION ORIGINALITY REPORT

HACETTEPE UNIVERSITY
GRADUATE SCHOOL OF SCIENCE AND ENGINEERING
TO THE DEPARTMENT OF NANOTECHNOLLOGY AND NANOMEDCINE

Date: 2.12./.2020

Thesis Title / Topic: FANO-CONTROL OF LOCALIZED AND NONLOCALIZED NONLINEAR RESPONSE

According to the originality report obtained by myself/my thesis advisor by using the *Turnitin* plagiarism detection software and by applying the filtering options stated below on 2../12../2020 for the total of ...100..... pages including the a) Title Page, b) Introduction, c) Main Chapters, d) Conclusion sections of my thesis entitled as above, the similarity index of my thesis is 10. %.

Filtering options applied:

1. Bibliography/Works Cited excluded
2. Quotes ~~excluded~~ / included
3. Match size up to 5 words excluded

I declare that I have carefully read Hacettepe University Graduate School of Sciene and Engineering Guidelines for Obtaining and Using Thesis Originality Reports; that according to the maximum similarity index values specified in the Guidelines, my thesis does not include any form of plagiarism; that in any future detection of possible infringement of the regulations I accept all legal responsibility; and that all the information I have provided is correct to the best of my knowledge.

I respectfully submit this for approval.

Date and Signature

Name Surname:	ZAFER ARTVİN
Student No:	N13145818
Department:	NANOTECHNOLOGY AND NANOMEDICINE
Program:	
Status:	☐ Masters ☒ Ph.D. ☐ Integrated Ph.D.

2.12.2020

ADVISOR APPROVAL

APPROVED.

Assoc. Prof.Dr. Mehmet Emre TAŞGIN

CURRICULUM VITAE

Name, Surname: Zafer ARTVİN

Place of Birth: ANKARA

Date of Birth:03-02-1977

Marital Status: Maried,two childeren

E-mail: z.artvin@gmail.com

Addres: Yukarı yurtçu mah. 4438. cad Odtü Toki sitesi 10 H blok d.15 Etimesgut/ANKARA

Education

High School: Yenimahalle Technical High School-Ankara,1995

B.Sc: Marmara University, Physics Education,1999

M.Sc: Middle East Technical University, Micro and Nanotechnology, 2012

Ph.D: Hacettepe University, Nanotechnology and Nanomedicine,2020

Work Experience

1999-2007 Physics Teacher-İstanbul and Ankara

2007-2020 Researcher- Central Laboratory/Middle East technical University